NASA/TM–20205009040

Implementation Concept of Operation for a Multi-Purpose Cassegrain Solar Concentrator, Micro-Spectrometers, and Electrostatic Neutralizers to Enable In Situ Construction Activities plus Lunar, Planetary, and Deep Space Science Exploration on the Moon

Sang H. Choi, Robert W. Moses, Cheol Park, Catharine C. Fay, and David R. Komar Langley Research Center, Hampton, Virginia

October 2020

NASA STI Program . . . in Profile

Since its founding, NASA has been dedicated to the advancement of aeronautics and space science. The NASA scientific and technical information (STI) program plays a key part in helping NASA maintain this important role.

The NASA STI program operates under the auspices of the Agency Chief Information Officer. It collects, organizes, provides for archiving, and disseminates NASA's STI. The NASA STI program provides access to the NTRS Registered and its public interface, the NASA Technical Reports Server, thus providing one of the largest collections of aeronautical and space science STI in the world. Results are published in both non-NASA channels and by NASA in the NASA STI Report Series, which includes the following report types:

- TECHNICAL PUBLICATION. Reports of completed research or a major significant phase of research that present the results of NASA Programs and include extensive data or theoretical analysis. Includes compilations of significant scientific and technical data and information deemed to be of continuing reference value. NASA counter-part of peer-reviewed formal professional papers but has less stringent limitations on manuscript length and extent of graphic presentations.

- TECHNICAL MEMORANDUM. Scientific and technical findings that are preliminary or of specialized interest, e.g., quick release reports, working papers, and bibliographies that contain minimal annotation. Does not contain extensive analysis.

- CONTRACTOR REPORT. Scientific and technical findings by NASA-sponsored contractors and grantees.

- CONFERENCE PUBLICATION. Collected papers from scientific and technical conferences, symposia, seminars, or other meetings sponsored or co-sponsored by NASA.

- SPECIAL PUBLICATION. Scientific, technical, or historical information from NASA programs, projects, and missions, often concerned with subjects having substantial public interest.

- TECHNICAL TRANSLATION. English-language translations of foreign scientific and technical material pertinent to NASA's mission.

Specialized services also include organizing and publishing research results, distributing specialized research announcements and feeds, providing information desk and personal search support, and enabling data exchange services.

For more information about the NASA STI program, see the following:

- Access the NASA STI program home page at http://www.sti.nasa.gov

- E-mail your question to help@sti.nasa.gov

- Phone the NASA STI Information Desk at 757-864-9658

- Write to:
  NASA STI Information Desk
  Mail Stop 148
  NASA Langley Research Center
  Hampton, VA 23681-2199

NASA/TM–20205009040

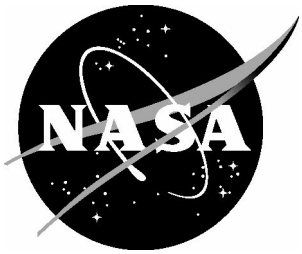

Implementation Concept of Operation for a Multi-Purpose Cassegrain Solar Concentrator, Micro-Spectrometers, and Electrostatic Neutralizers to Enable In Situ Construction Activities plus Lunar, Planetary, and Deep Space Science Exploration on the Moon

Sang H. Choi, Robert W. Moses, Cheol Park, Catharine C. Fay, and David R. Komar Langley Research Center, Hampton, Virginia

National Aeronautics and

Space Administration

Langley Research Center
Hampton, Virginia 23681-2199

October 2020

Acknowledgments

The authors would like to express their appreciation to Mr. Gerald Sanders (NASA Johnson Space Center) who leads NASA's Systems Capabilities Leadership Team for In Situ Resource Utilization. Jerry provided valuable comments on approaches for identifying and collecting raw materials on the Moon and Mars. His comments guided our thinking on construction feedstock creation. The authors would like to thank Dr. Robert P. Mueller, Senior Technologist of NASA Kennedy Space Center whose experiences in laboratory-scale building of landing pads and other infrastructure on the Moon helped focus our priorities on technology development. The authors would like to thank Dr. Paul Hintze for reviewing the document as well as publishing some of his work that is referenced herein. Building a strong relationship with these experts has been extremely valuable.

Available from:

NASA STI Program / Mail Stop 148
NASA Langley Research Center
Hampton, VA 23681-2199
Fax: 757-864-6500

Implementation Concept of Operation for a Multi-Purpose Cassegrain Solar Concentrator, Micro-Spectrometers, and Electrostatic Neutralizers to Enable In Situ Construction Activities plus Lunar, Planetary, and Deep Space Science Exploration on the Moon

Sang H. Choi, Robert Moses, Cheol Park, Catharine Fay, and David R. Komar

SUMMARY

The ability to utilize regolith would support human missions to the Moon and Mars by both stabilizing the surface as well as the use of indigenous resources. Precision landing requirements include surface stabilization to prevent damage or contamination due to regolith projectiles as a result of plume interaction with regolith. The use of indigenous resources rather than hauling materials from Earth appears to be economically a palatable option by converting indigenous resources to usable products. However, such activities have new technical challenges to overcome the issues related to lunar environmental conditions, a wide range of temperature fluctuation, extremely high vacuum, and electrostatically charged fine regolith dusts. For both the regolith sintering and extraction of resources onsite, a Cassegrain solar concentrator was studied for not only sintering lunar regolith into a hardened stabilized surface, but also other multiple applications. This report illustrates a Cassegrain solar concentrator that has multi-functional capabilities for space missions. Proper design and implementation of high-performance lightweight composite materials for the primary mirror of the Cassegrain concentrator can offer multiple capabilities to be performed on the Moon. The multiple applications studied with Cassegrain concentrators are (1) Solar sintering for landing pad and habitats, (2) Harvest of volatiles: H_2O, O_2, H_2, and He-3, (3) Space antenna for telemetry and telecommunication, and (4) Space telescope with 20-meter aperture that exceeds the space telescopes to date in terms of the State-of-Art (SOA) in resolution and aperture diameter. In this study, a key emphasis was placed on the NASA Langley-developed boron nitride nanotube (BNNT) nanocomposite technology which is ideal for the segmented primary mirror structure of the Cassegrain system because it promises a very low coefficient of thermal expansion (CTE) and negligible Poisson ratio. Also, BNNT nanocomposites offer several noticeable benefits, such as light weight, radiation shielding capability, and mechanical strength for structural applications.

Additionally, the NASA Langley-developed bullet-like micro-spectrometer and electrostatic power generator were reviewed for mineral mapping applications and electrostatic power generation and dust mitigation from electrostatically charged regolith.

I. INTRODUCTION

The first step to a Deep Space Gateway is lunar exploration that plans to establish lunar habitats and onsite production facilities for water, propellants and raw construction materials under the In-Situ Resources Utilization (ISRU) program. To initiate and sustain the activities of ISRU on the Moon, several challenges need to be identified and clarified with technical understandings and eventually to suggest potential solutions as precursory preparation guidelines. Under the defined guidelines, ISRU infrastructure is planned by introducing the concepts of functional elements, designs, fabrications, constructions, and validation tests considered under a full consideration of lunar environmental conditions prior to deployment. Prior to the establishment of lunar bases with habitats and onsite production facilities of water, oxygen, propellants, and raw construction materials, we anticipate numerous shuttle operations of cargo transportation from Earth to the Moon by rockets. In such operations, major problems and technical issues and needs related to the flying dust of regolith by rocket plume, the harvest of volatiles and water molecules, the mining and production of raw construction materials must be illustrated with accurate analyses. The Apollo era database related to lunar environmental

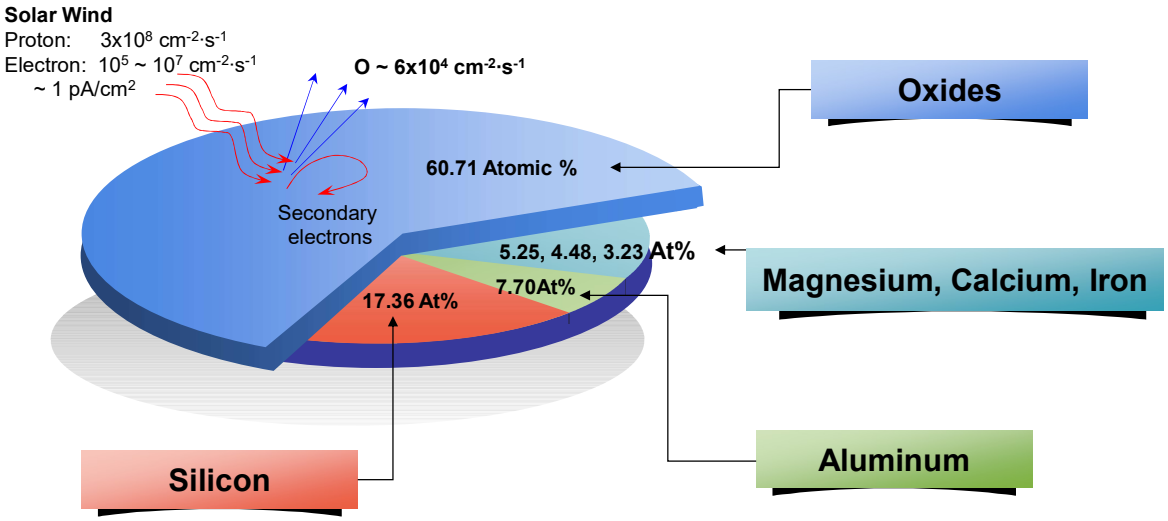

Figure 1. Lunar dust composition.

conditions identifies several challenges to be properly considered, such as the interaction of rocket exhaust gas plume and regolith, the contamination by electrostatically charged fine regolith dusts, the harvesting of lunar volatiles at extremely high vacuum, and so on. The landing and launching of rockets carrying astronauts and payloads on lunar surface create repeatedly rocket plume interaction with the surface regolith. An abrasive cloud of ejecta and electrostatically charged regolith dust harms nearby equipment and crew during launch and landing operations. Regolith is lunar soil with very fine particles, negatively charged [1], and can be easily dislodged at high velocity and spread widely by the blast wave of rocket plume due to the composition of very fine particles (4μm - 250μm) [2], low gravity, and very high vacuum (~ 10^{-12} torr). Figure 1 shows a rough estimation of lunar soil composition. The major components of the regolith are oxides of silicon, aluminum, magnesium, calcium, iron, and others, comprising approximately 60 atomic % (At%) of pure elements and 40 At% of oxygen. The remainder are pure elements, containing 17.36 At% silicon, 7.70 At% aluminum, 5.25 At%

magnesium, 4.48 At% calcium, 3.23 At% iron, and the remainder is other elements [2]. These oxides interact with the incident high energy particles (protons and electrons) of solar wind and are split into pure elements and oxygen atoms.

As stated previously, the lunar exploration and colony development would require many operations as depicted in Fig. 2. Low gravity and no atmosphere on the Moon can allow very fine and electrostatically charged lunar dust to easily migrate or displace to great distances and pose great difficulties on lunar missions. During the Apollo 17 lunar mission, charged lunar dust was a major hindrance, as it was attracted to the astronauts' spacesuits, equipment, and the lunar buggies [3, 4, 5, 6, 7]. Dust that accumulated on the spacesuits, including the vision goggles, also caused reduced visibility for the astronauts, and was unavoidably transported inside the spacecraft where it caused respiratory irritation [8]. Therefore, the dust mitigation has since become a key technology requirement on lunar exploration. The construction of a landing

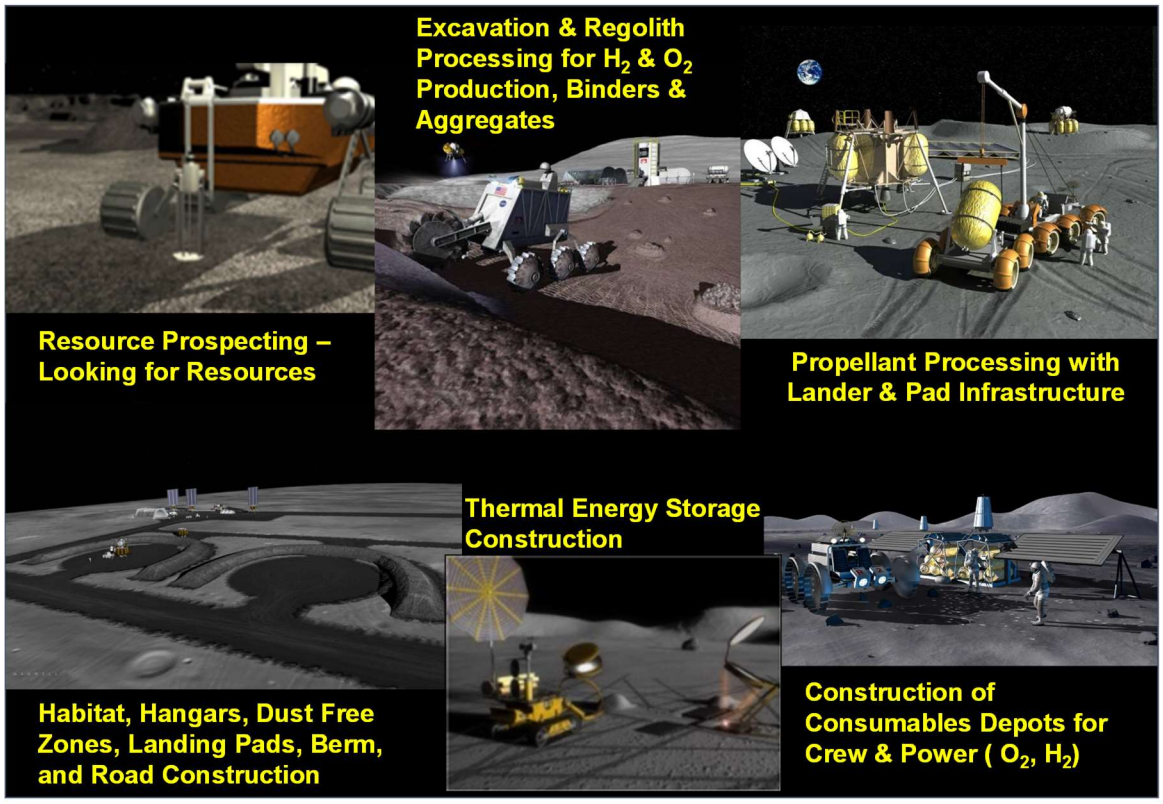

Figure 2. Artist's concept of lunar exploration. (credit NASA)

pad necessary for safe and effective landing and launching operation of rockets avoids the rocket plume blasted dusts.

Several construction techniques are available for constructing landing and launch pads on the lunar surface using natural resources there. In Situ Resource Utilization (ISRU) tools and equipment that greatly reduce demand on mass and energy and can be brought from Earth are most desirable for reducing costs.

The lunar surface offers some advantage over the Martian surface with respect to energy. Solar power is far greater in direct sunlight on the lunar surface than on the Mars surface, due to its proximity to the Sun. However, Mars is vulnerable to dust clouds due to the presence of still-

thin atmosphere (0.6% of Earth atmosphere) and gravity (3.7 m/s^2) that offer plenty of resistivity against flying particles unlike on the Moon where flying particles can fly over long distance in vacuum and low gravity. Because of a CO_2 atmosphere and abundant subsurface frozen (water) ice lakes, Mars offers slightly more construction materials than the lunar surface. However, both offer regolith that is easily accessible and pliable with the right amount of energy.

The focus of this technical memorandum (TM) is to describe the In-Situ Construction process that would be beneficial for sustained Lunar exploration and to illustrate how it differs from previous research.

Solar sintering is a promising technique since it gets its power from the Sun (1353 W/m^2). In 2008, Hintze et al. demonstrated the use of solar sintering to melt the grains of lunar regolith simulant and fuse them into one structural element (tile or brick) [9]. They used a large Fresnel lens with a one square meter collection area mounted on a frame (Figure 3). The solar concentration by the lens is pointed downward to the surface of regolith simulant and rasters across a surface. The highest measured temperature at the spot of the solar concentrator has been 1350°C, higher than is necessary to melt JSC-1A lunar simulant. Solar concentrators can be made with an array of lightweight Fresnel lenses which are inexpensive and a relatively simple technology. Similar techniques were considered to develop entry heat shields [10]. The ability to fabricate Fresnel lenses depend on size and cost. Currently, the largest available size of a Fresnel lens is 1 m^2 shown in Fig. 3. When the size is increased, the number density of Fresnel gratings must be increased in order to reduce the unfocused (or undiffracted) transmission loss.

Figure 3. The 1 m^2 solar concentrator built at NASA KSC. (credit NASA)

In the study done by Hintze et al., sintered samples ranging in thickness from 2.5 to 6 mm were tested and found to have strengths between 130 and 310 psi. Because gravity on the moon is 1/6 that of earth, structural dead loads will be reduced by 5/6 and components should have 6 times the load bearing capacity of conventional materials on Earth. Using a 1/6 reduction in thickness, the moon's highways could be 2.6 to 4.3 cm, as compared to the 15 to 25 cm used on Earth [11, 12]. The sintered samples are considerably thinner than that value; however, the bearing strengths of these samples are in excess of the Apollo lunar module bearing pressure of 4.6 kPA (0.67 psi) meaning they would support the dead weight of the landers. This does not suggest that they would withstand the force from the ignition of the rocket or the forces that might occur if a footpad hit at an angle and did not properly distribute its weight.

II. SITE FOR HABITATS AND EXPLORATION

II-1. Site Development for Lunar Base

Future lunar posts considered as bases for cislunar activity and/or a mid-point station for Mars exploration will need natural resources, such as oxygen and water, for sustaining the post and providing propellants needed for the rockets in- and out-bound transportation for deep space missions. Accordingly, the site selection for lunar base can be made by several important factors in conjunction with the scenario of exploration mission. The terrain and location for lunar posts must be easily accessible from orbit and offer easy operation of rovers and construction equipment (Fig. 2). It should also be close to usable resources that are easily accessible for mining.

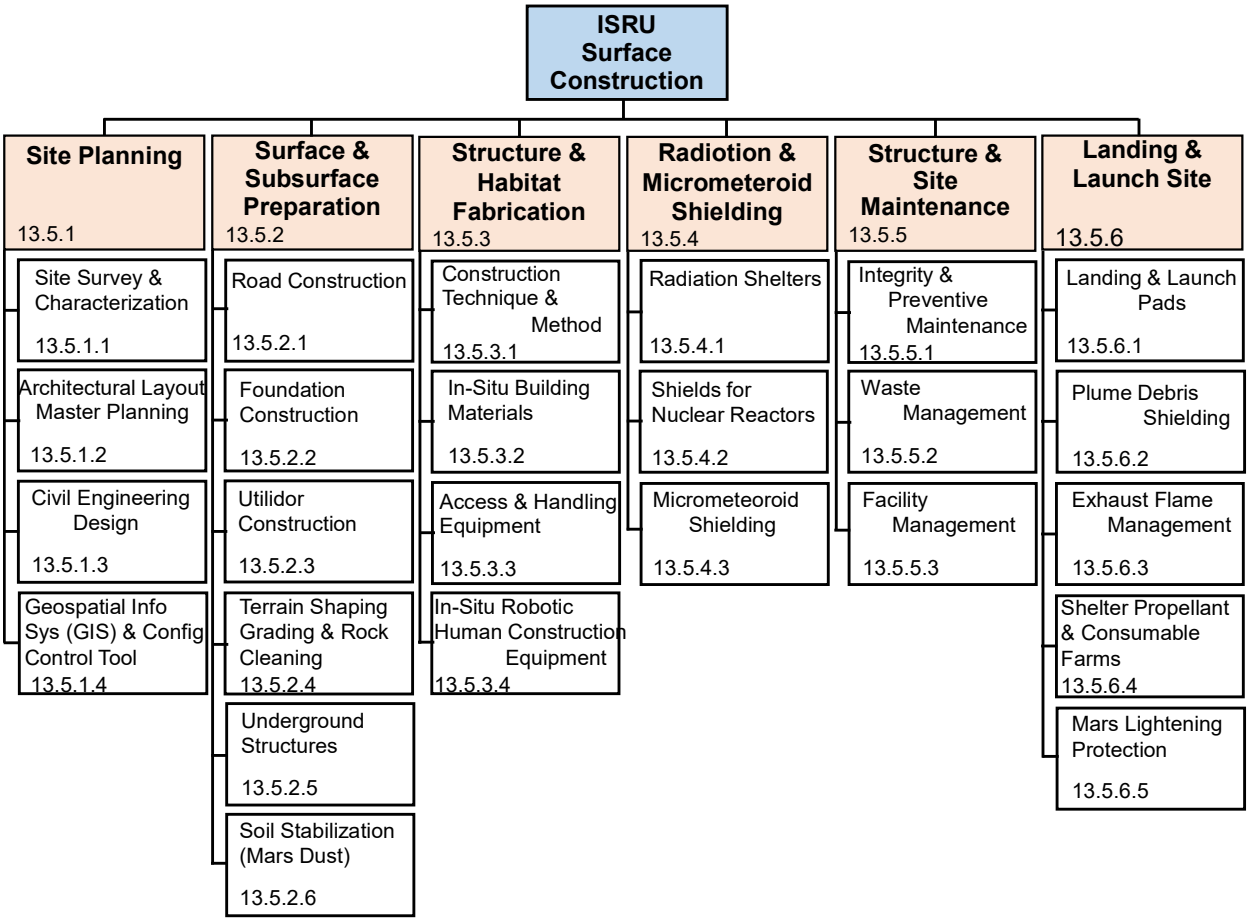

Figure 4. Lunar surface construction plan as a part of ISRU.

Construction tasks will constitute over 80 percent of the surface activities based on volume of regolith to be moved [13]. The lunar construction tasks, as shown in Figure 4, need to have (1) the site planning that includes the site survey and characterization and the architectural layout and design of master lunar colony, (2) the ground works for road, construction foundation with shaping, grading, and rock cleaning, and soil stabilization with dust mitigation, (3) the structure and habitat fabrication with in-situ building materials, (4) the protective shielding against micro-

meteoroids and radiation, (5) the maintenance of structure and site, including waste management, (6) the development of landing and launch pads for preventing flying dusts and debris from rocket plume, and (7) the development of propellant and consumables storage.

Lunar water is thought to exist in the form of ice within the permanently shadowed regions of the north and south poles of the moon [14, 15]. Based on the Clementine probe [14] and the Lunar Prospector [15], the permanently shadowed areas are estimated to be around 14,000 km^2 [16]

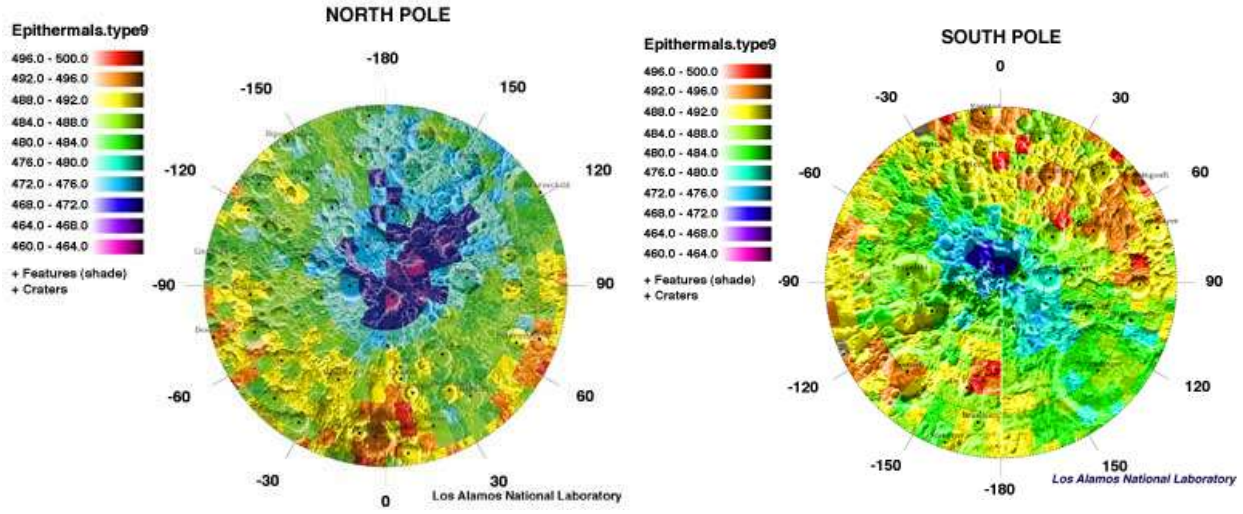

Figure 5. LP Neutron Spectrometer data from the north and south poles showing evidence of water ice. North pole - dark blue to magenta, and South pole - dark blue to purple. [17]

and could contain volumes of surface lunar ice on the order of 1~3 km^3 [17]. Figure 5 shows the ice caps on the north and south poles of the Moon measured by the neutron spectrometer of Lunar Prospector probe [17].

Water can exist also on the Moon as chemically bound hydrates and hydroxides to lunar minerals [18] or absorbed water into lunar soil [19]. If mining of other needed materials is required, then the process of extracting water and other volatiles could be operated in an organized fashion. Acquiring samples and analysis, mining, sorting and rectifying, and storing because this process requires a large number of equipment and facilities. The same would be true when moving regolith during construction tasks. Processes for both mining and construction could be coordinated to minimize energy and increase efficiency of surface operations.

The first construction phase of lunar posts could occur before astronauts and cargos are landed on the designated location of the moon as indicated in Figure 4.

II-2. Resources Identification by Bullet-like Micro-Spectrometer

Identifying usable accessible resources on the Moon will require closer examinations that cannot be done effectively by orbiters. Since construction processes involve contact with the

regolith where the resources reside, integrating some sensing, selection, sorting, collection, and storage concepts concurrently may be prudent. However, in some cases, some resources may need identification in advance of any construction activities. Verifying the possible locations of mission-needed materials, such as water, oxides, and helium-3, could be done prior, and be a necessary requirement for site selection. The survey of naturally existing water and minerals on the surface of the Moon are limited within the mobility ranges of rover and astronauts. Some hopper concepts are being considered for surface mobility to increase the range of exploration on the lunar surface [20]. The hopper vehicle may offer utility for conducting resource identification.

Micro-Spectrometer: Assays of soil composition on the Moon, Mars, or asteroids are one of the essential exploration tasks. Since the Langley-invented micro-spectrometer [21-24] has a tiny embodiment with a nanometer resolving power of spectral signal, it is possible to build a bullet-like consumable micro-spectrometer that can be shot out to remote and wide locations, including non-accessible steep hillsides of mountains and deep craters. The device can be shot by astronauts, from the platform of rovers, or even satellites for wide area coverage of soil assay. This device can be also installed on rover tires, under the astronaut's shoes or cane stick. The bullet-like consumable micro-spectrometer can penetrate into soil to spectrally identify the components of soil, such as water, He-3, or other minerals. The signals of soil assay data are transmitted to a mother station through telemetry system.

The consumable micro-spectrometer bullet consists of micro-spectrometer optics with a burst-mode LED UV light source, a super-capacitor with control electronics, and telemetry electronics. The micro-spectrometer was successfully developed for neural probe applications to monitor the emission of dopamine in a synaptic reaction under the external funding through the NASA Space Act Agreement (SAA) with Gacheon Medical School (SAA #26160) [25].

The assay of lunar, Martian, or asteroid soils can help identify biosignatures, water, and minerals using spectral responses of chemical components in soil through a spectrometer. Most conventional spectrometers are based on the Fraunhofer diffraction principle, which requires a long path-length and high grating line density for high resolution. Such spectrometers are too bulky and heavy for space applications. The proposed bullet-like micro-spectrometer is built, instead, with the Fresnel diffraction principle which allows miniaturization for very tiny and lightweight embodiment as shown in Figure 6.

A new concept proposed here is the development of consumable bullet-like devices, each containing a micro-spectrometer, a burst-mode LED UV light source, a super-capacitor, control electronics, and telemetry electronics for identifying the biosignatures of water, or minerals to meet the 2014 NASA Technology Roadmap, In Situ Instruments/Sensors 8.3.3.6, which was released on July 28, 2014. Once a bullet-like micro-spectrometer penetrates the soil, an intensive deep or vacuum UV light from a burst-mode LED powered by the super-capacitor illuminates the target soil in a pulse mode to generate fluorescent or luminescent emission by a singlet or triplet quantum transitions from the illuminated target material, as shown in Figure 7. The fluorescence or luminescence emission spectra is captured and analyzed for the spectrally resolved signature of chemicals by the micro-spectrometer through a Fresnel grating. These measured spectral data are, then, sent to the mother station through an onboard telemetry system. The devices can be deployed to distant and wide areas using an astronaut-held gun or at a platform of rover as shown in Figure 8 or self-propelled by a tiny rocket attached at the rear end of micro-spectrometer. The devices can also be deployed from an orbiting satellite, allowing a wider area and a deeper penetration for soil composition at a lower depth.

We have developed the micro-spectrometers under the Space Act Agreement (SAA #26160) funding (see Figure 9). There are several critical elements to be refined for a deployable class of micro-spectrometer bullet.

Avalanche photodiode (APD): Most of charge-coupled device (CCD) or complementary metal-oxide semiconductor (CMOS) photo sensors are not sensitive enough to capture a low flux density of photons in a signal stream. Accordingly, it would be very desirable to enhance the sensitivity of the photo-sensor by using an array of avalanche photodiode to be integrated into micro-spectrometer for better chromatic resolution.

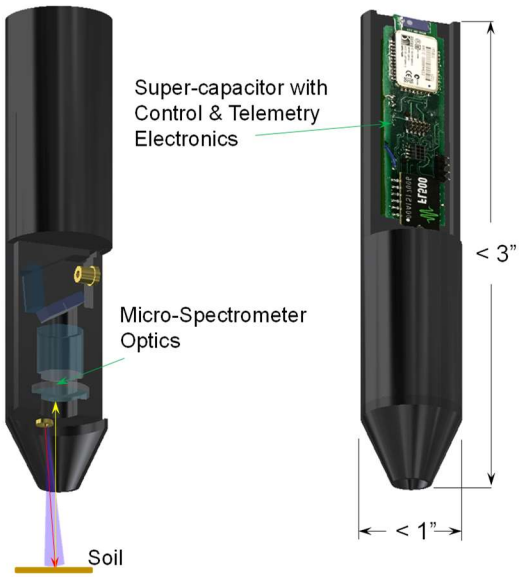

Figure 6. Langley invented micro-spectrometer was developed under the support of SAA #26160 and meets NASA Roadmap 8.3.3.6

Super-capacitor: The power required to drive a burst-mode of LED to emit a short wavelength requires an energy storage device that releases energy in a pulse mode at a short period of time. The power is also shared to operate APD and telemetry system.

A barrel of shooting gun or booster rocket: A bullet-like micro-spectrometer can be launched by compressed air just like BB gun or propelled by its own tiny rocket booster attached at the rear end of micro-spectrometer bullet. While the bullet-like micro-spectrometer passes through the barrel of shooting gun, it is electromagnetically charged to store the power into a supercapacitor. A portion of the barrel has built-in multiple rings of magnets that enable a charging coil of bullet-like micro-spectrometer to generate electrical power when it passes through it.

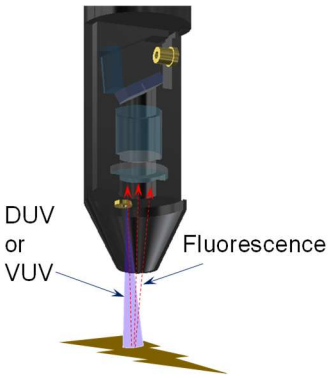

Figure 7. DUV or VUV initiated fluorescence or luminescent emission.

A telemetry system for data transmission: The refinement of micro-spectrometer systems illustrated above will raise the deployment readiness level to TRL 6. Before onsite deployment, this device configuration will be tested for validation and device readiness level on volcanic ashes or other soils. Numerous soil assay experiments will be compared with the spectral database of soil organic and inorganic components compiled by U.S. Geological Survey (USGS) for validation of the device.

Once the validation process is over, the micro-spectrometer bullet with gun or launching device will be prepared for deployment packaging as a final process.

In general, the concept of a micro-spectrometer bullet is new and innovative in terms of the cost to build and the broad deployment capability for soil assay. The innovativeness can be identified by the following facts:

- Micro-spectrometer is a NASA LaRC invented technology [24]
- It was developed as a neural probe under the SAA #26160. It was proven successfully by monitoring dopamine in the lab [25].

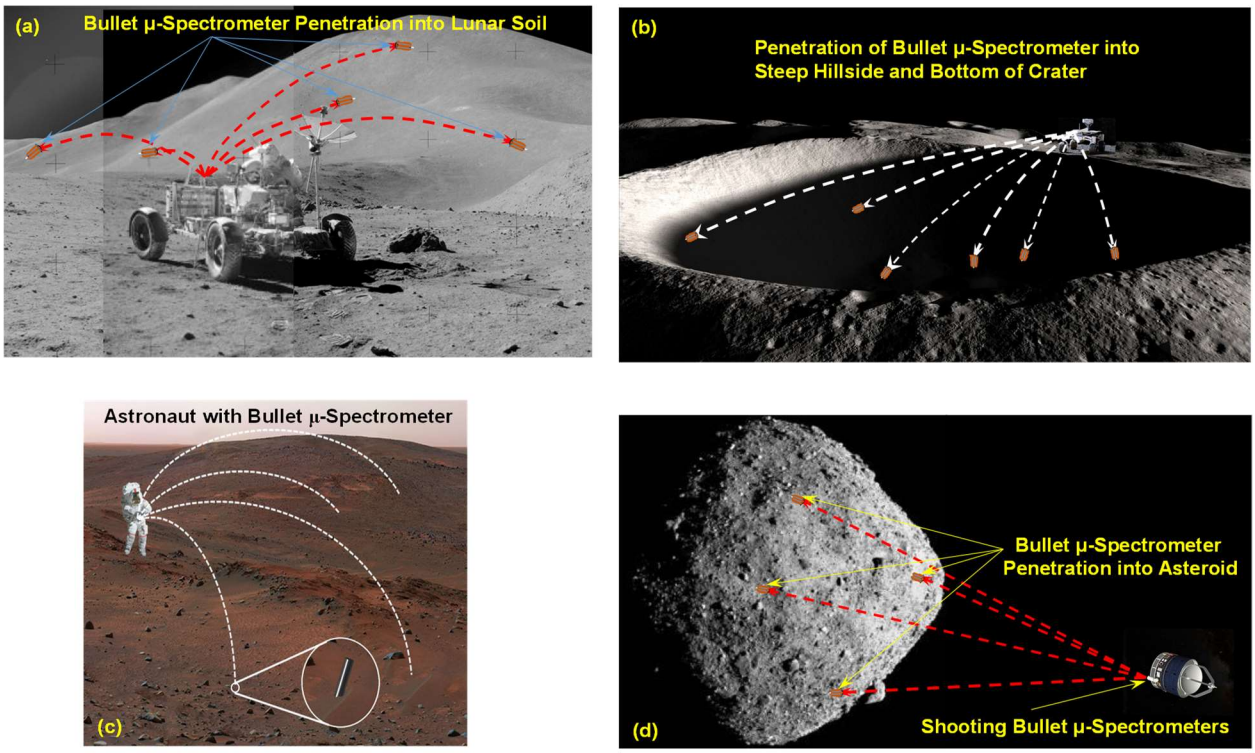

Figure 8. Bullet-like consumable micro-spectrometers are shot out broadly to assay organic and inorganic components of Lunar/Mars/Asteroids soils.

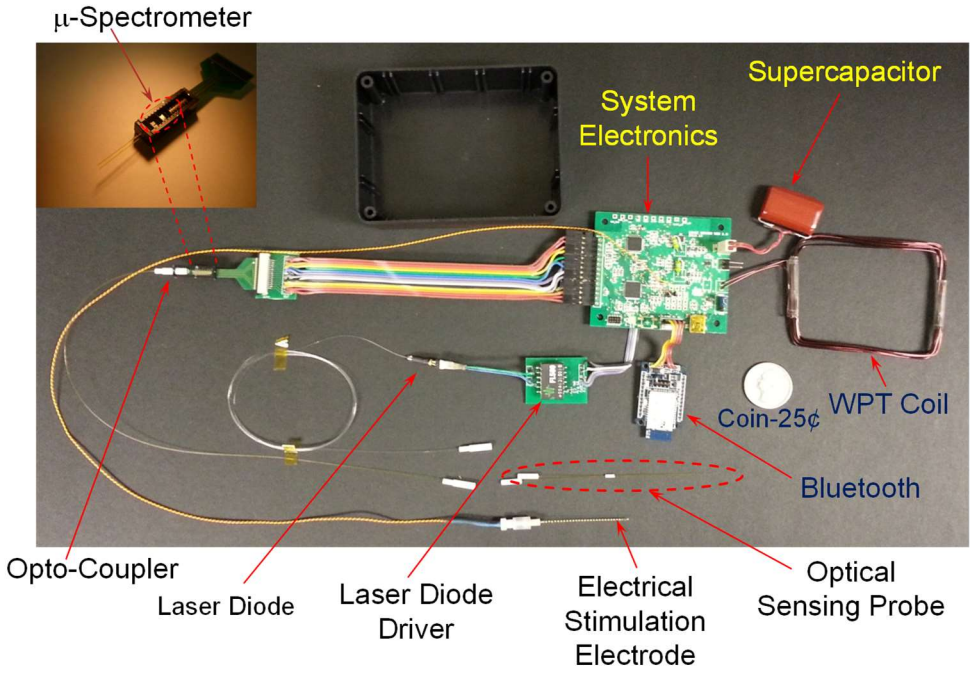

Figure 9. A micro-spectrometer built as a test article with electronic subsystem for monitoring dopamine emission in a synaptic reaction of brain.

- Consumable bullet-like micro-spectrometer is a new design and new approach to distribute

to remote locations by a gun for wide area assaying simultaneously.

- A convenient exploration tool for future space missions, i.e. Lunar and Mars soil assay, survey and assay of permanently shadowed regions (PSR), such as deep craters, asteroid as shown in Figure 8(d).

II-3. Dust Mitigation and Electrostatic Power Generation (ESPG)

The adhesive and abrasive lunar dust that is composed of very fine (4~250 μm in diameter) and electrostatically charged particles impose serious problems on various lunar missions. Such fine dust can easily fly away by charge attraction or repulsion and adhere to clothing and equipment (Figure 10), reducing external visibility on landings, and causing difficulty to breathing and vision within the spacecraft [5, 7]. Some dust problems are tabulated in Table 1.

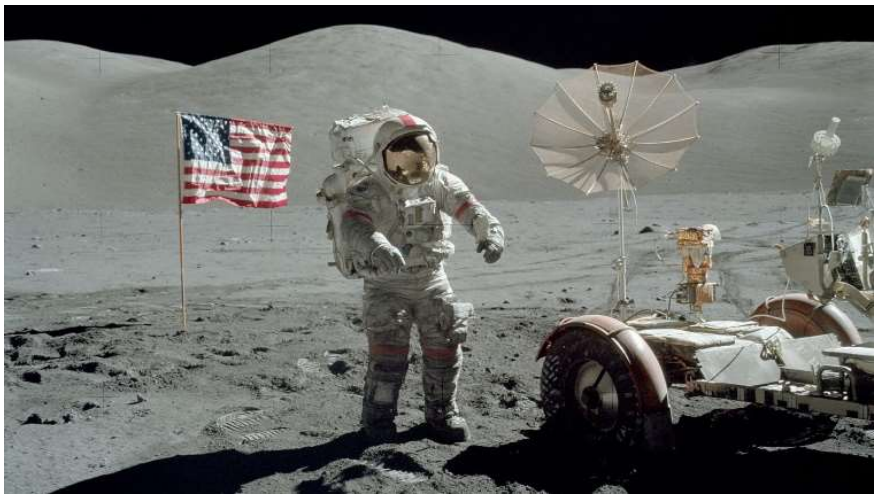

Figure 10. Astronaut's suit and rover were covered by lunar dust (Apollo 17). (credit NASA)

Dust mitigation on lunar surface is a serious task to be prepared well ahead of any mission operations. Table 1 shows the significance of lunar dust contamination on those components of various systems for onsite operations on Moon and Mars. The main cause of dust contamination is due to the fine size of regolith and the electrostatic charge density of dust.

Table 1. Contamination vulnerability by fine dusts of lunar regolith

System \ Components	*air filters*	*rotating shafts*	*sliding shafts*	*optics & PV panels*	*radiator reflector panels*	*pressure seals*	*exposed surfaces*	*electrical connectors & switches*
Spacesuits	✹			✹	✹	✹	✹	✹
Air Locks	✹	✹				✹	✹	
Exploration Vehicles	✹	✹	✹	✹	✹	✹	✹	✹
Habitats	✹	✹	✹	✹	✹	✹	✹	✹
Power		✹	✹	✹	✹	✹	✹	✹
Antenna		✹	✹	✹	✹	✹	✹	✹
Robots & Rovers		✹	✹	✹	✹	✹	✹	✹

The lunar regolith is composed of a finely pulverized nano- to micro-size particles resulting from millennia of constant meteoroid bombardment. Both the lunar vacuum and the magnetic field contribute to the negatively charged, levitating dust layers produced from the persistent bombardment of electrons and protons from the solar winds [27]. The stream of impinging solar wind on the lunar surface is a combination of protons (10^8 $cm^{-2}s^{-1}$ ~ 10^{13} $cm^{-2}s^{-1}$) [28, 29] and electrons (10^4 ~ 10^7 $cm^{-2}s^{-1}$) [30, 31]. These particles in flux modify the regolith in a variety of ways, including space weathering; electric charging; implantation; chemical alteration; and sputtering, which is typical for the nature of the lunar environment, particularly in permanently shadowed regions [32, 33]. The three major populations of impinging particles are from the solar wind, the episodic solar energetic particles (SEPs), and galactic cosmic rays (GCRs). SEPs and GCRs with several keV to MeV level of energy [30, 31] can penetrate regolith to a range of depths. The SEP events are known to be associated with extreme surface charging of up to ~ 4 keV negative [34, 35]. High fluxes of protons with a high impact velocity of ~ 1 keV are capable of breaking oxides apart to create atomic oxygen up to 6 x 10^4 $cm^{-2}s^{-1}$ flux density level and secondary electrons from oxides [36] and form water molecules with separated oxygen [34] and/or some (~1%) of the impinging protons are reflected from lunar surface [37]. It is also reported that SEP from 50 keV to 5 MeV [30, 31, 35] can penetrate a few centimeters to a meter of lunar soil [38] generating negative potentials as large as ~ 4.5 kV [35]. The maximum charge on the lunar surface was also estimated to be several thousand volts [39]. Impinging electrons onto very fine regolith particles over long periods of time increases negative charge accumulation, since most protons with a larger cross section are removed from the regolith by the repeated collisions from the accompanying helium in the solar wind [40]. Helium is 4 or 5 times more abundant in solar wind and has a large cross-section for proton-helium (H-He) collision [41]. Thus, negative charge accumulation in the lunar regolith by the continuous stream of impinging electrons creates high electric fields of electrostatic charge. In short, the negative charge processes can be described by (1) photoelectric emission by UV radiation at wavelengths < 200 nm (~ 6 eV) during the lunar day, leading to positively charged grains, but at a very low level [42, 43], (2) electron or ion collisions during the lunar night, generally leading to negatively charged grains with energetic electrons (< 100 eV) [44], (3) secondary electron emission by the solar wind electrons (400~750 km/s, 1.6 keV~300 keV, 105~107 $cm^{-2}\cdot s^{-1}$) [30, 31, 45, 46], and (4) triboelectric charging of dust grains by contact charging processes [47].

In the contact charging process, electrons are transferred from a solid material with a high work function to one with a lower work function. The Earth is surrounded by a magnetic field that is trapped inside a conducting plasma tail that stretches well beyond the Moon's orbit. The Earth's magnetrospheric tail points away from the Sun due to the high-speed ions streaming along with the solar wind. The movement of the Moon through the ionized plasma affects the materials in the lunar regolith. Electrons accumulate and produce a negative charge on the ultra-fine dust particles, causing them to repel each other and drift off the surface. The faint glow on the lunar horizon is most likely caused by the levitating dust because the Moon has no atmosphere, and so no collision for charge dissipation. Therefore, the electric charges have greater impetus.

The electric field itself affects machinery on the surface: this process has been demonstrated to be a leading cause of spacecraft failures in space missions [48]. Surface electric fields had few demonstrably significant effects on the Apollo missions, but these missions were conducted with limited exposure to the terrestrial plasma sheet or SEP events, and astronauts only experienced the lunar surface in the relatively benign surface charging environment in the morning sector,

where electric fields were therefore expected to remain at relatively low levels. In a more energetic plasma environment, surface electric fields might have more significant effects, especially considering the abrupt changes in surface potential often encountered. In addition, surface electric fields also likely contribute to dust charging and transport. There is substantial observational support for dust levitation a few meters above the surface [49], and some evidence for dust transport to much greater altitudes [50]. Lunar missions for exploration and resource exploitation potentially face disasters or may be severely limited without a means to neutralize these charges.

In this report, we describe a device to generate electrical power from the charged lunar surface, while simultaneously neutralizing and mitigating the charged particles through capacitive collection or coupling of electrons [2]. The device, called electrostatic power generation (ESPG), could be a valuable asset for human exploration and lunar resource utilization by harvesting electrical power, while alleviating problems associated with electrostatic charging [51, 52]. The ESPG is differentiated from electrostatic generations, such as the Van de Graaff generator [53], which is generally known as a very high electric potential generating device [54]. The electrostatic generator is designed to accumulate electric charges on an isolated conducting body in order to create a very high voltage. On the other hand, the ESPG concept is to collect and feed the accumulated electric charges into power circuit for useful power output [51, 52, 55]. There are several different versions of electrostatic power generators [55, 56] categorized by the sources of electret, such as tribo-electric charges [53, 56, 57, 58] and vibration or mechanical [59]. Details of electrostatic energy harvesting technology are well illustrated in a book specifically dedicated on triboelectric devices for power generation [60]. The ESPG

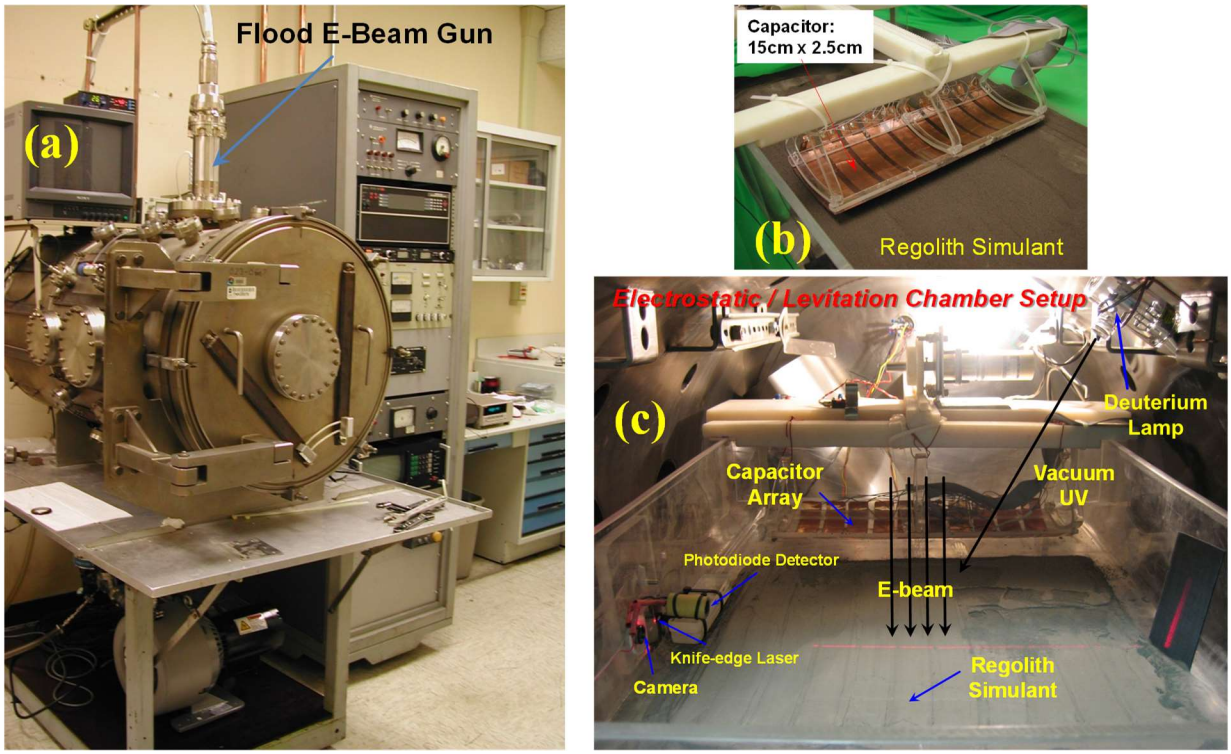

Figure 11. (a) Test chamber with a flood electron gun. (b) An array of capacitors on the regolith simulant. (c) Experimental setup inside the chamber.

studied in this research uses homocharge electret with implanted electrons by space plasma which is similar to the description in the Figure II-5 of [55]. This research demonstrates the feasibility of a device function that collects the charges for generating useful electrical power which can be fed back to lunar vehicles and equipment while neutralizing the charge on the lunar soil. The amount of power generated is mainly determined by the available surface charge, the collector area, and collection speed over the lunar soil surface. The collector consists of a thin-film array of capacitors that are continuously charged and sequentially discharged using a time-differentiated trigger discharge circuit to produce a pulse train of discharge for DC mode output.

ESPG Experiment: The test facility for power collection from electrostatic charged lunar regolith, shown in Figure 11, was set up with a vacuum chamber with an attached flood electron beam gun. This chamber holds a test bed of lunar regolith simulant on which a 30-cm wide diameter e-beam is incident for developing charges and a flexible array of capacitors are run over by an electric motor to collect the charges from the electrostatically charged lunar simulant.

For test purposes, lunar regolith simulant (Planet LLC, type JSC-1A) was acquired and ground into very fine particles using a tumbler, and sieved to obtain a narrow distribution of particles

Table 2. Comparison of ESPG test chamber and Moon environment.

	Moon	ESPG Chamber
Charged Surface (Radiation)	Solar wind, solar energetic particles, galactic cosmic rays	Flood beam electron gun
Ambient Pressure	10^{-12} torr (night) to 10^{-10} torr (day)	$10^{-6} \sim 10^{-5}$ torr ($<10^{-5}$ torr for e-beam gun operation)
Surface Particle	Lunar Regolith	Lunar regolith simulant (Planet LLC, type JSC-1A)
Size	< 45 μm (40wt % of soil)	700 nm ~ 1 μm
Property (dielectric)	Dielectric (insulator)	Dielectric
Property of the surface	- Extremely fine - Electrostatically charged particles - Electrostatic dust transport	- Extremely fine - Exposed to high electric field - Low humidity
Magnetic field	No global field, Isolated paleofields, (magnetic field strength: $3x10^{-9}$ ~$3.3x10^{-7}$ tesla)	No additional magnetic field except earth magnetic field (but shielded)

selectively between 700nm and 1μm, and dried in a vacuum oven at 250°C for hours to remove moisture and oxygen. Table 2 shows the comparison between the experimental chamber conditions for the electrostatic power generator (ESPG) system test and the moon environment.

A sample of the simulant was sandwiched between two aluminum foil plates and compressed into a 1.2-cm diameter disk using 103 MPa pressure to estimate capacitance of the simulant. A capacitance of approximately 110 pF/m was measured with a Keithley LCZ Meter, model 3330. Figure 11(a) shows a test chamber of the electrostatic power generation system. This chamber was kept under a vacuum pressure of 10^{-5} to 10^{-6} torr for a stream of electrons from an e-beam gun to pass through without being scattered by remaining gas elements within the chamber. A flood e-beam gun (Kimball Physics Inc. models EGF-6115 and EGPS-6115) attached to the top port of the chamber in order to guide the e-beam down to the simulant was used to electrically charge the fine particles of lunar soil simulant by attaching electrons under a vacuum condition

within the chamber. The test chamber was basically designed for the e-beam to charge the simulant negatively and then for a capacitor array to collect electrons from negatively charged simulant while sweeping over the negatively charged simulant surface as shown in Figure 11(b). The collected charges were converted into modulated DC power. An array of single-layer, flat capacitors was designed and fabricated to sweep over a wide area of lunar simulant securely to neutralize and mitigate negatively charged dust while generating electric power. An approximately 2-cm thick layer of regolith simulant was evenly spread over the bottom surface of the acrylic tray which was placed inside the chamber as shown in Figure 11(c). The charge

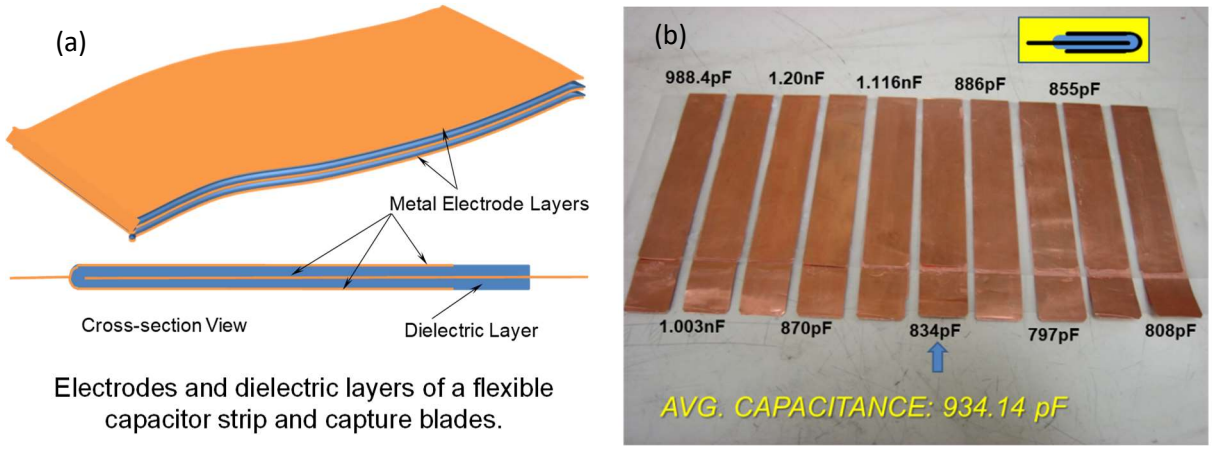

Electrodes and dielectric layers of a flexible capacitor strip and capture blades.

Figure 12. Flexible capacitor strips made for electron capture.

collection capacitor was fabricated with a 30-cm wide and 30-cm long thin copper plate and dielectric film. The thin copper plate was covered by a dielectric film and both layers were folded in half to sandwich a 15-cm long copper plate. In this way, the copper plate in the middle is wrapped by the folded dielectric/copper layers as shown in the cross-section view in Figure 12 (a) and in the inset of Figure 12(b).

A high dielectric material was used and sandwiched by metal layers to hold and sustain a very high voltage charge. The array of capacitors was made on a flexible membrane patch to increase the contact to an uneven surface of lunar soil. The capacitor arrays used in the test were made with a Polyvinylidene Fluoride (PVDF) membrane which has a static relative permittivity of 10 at room temperature under 1 kHz. The average capacitance of each capacitor was 0.934 nF. The array of capacitors was mounted on a carriage driven by a variable-speed DC motor.

The chamber was filled and purged with argon several times and pumped down to maintain 3 x 10^{-5} torr vacuum pressure through which electron beams were allowed to pass to charge the regolith simulant at the tray. At pressures higher than 3 x 10^{-5} torr, most of electrons are scattered by the air molecules. Lowering the vacuum pressure below 3 x 10^{-5} torr with a Sargent Welch TurboTorr 3133 turbopump, backed by a Varian Triscroll 600 roughing pump, was very difficult due to the outgassing from the very fine particles of simulant. The electron gun was operated at or near the peak output with a beam voltage set from 1kV to 25kV, giving an

emission beam current with the following equation y=1.1174x-1.1911, where x is filament voltage. The grid voltages of 0V and 100V were used to turn on and off the electron beam, respectively. A PC Oscilloscope (Pico Technology, Ltd. PicoScope 4000 Series) measured capacitor discharge voltages.

After charging the simulant with the flood e-beam flux, the e-beam gun was turned off, and the capacitor carriage was run over the simulant to collect the charges. The collection circuit with a total of 10nF capacitance was located outside the test chamber. The stored voltage was measured at points A and B (Figure 13).

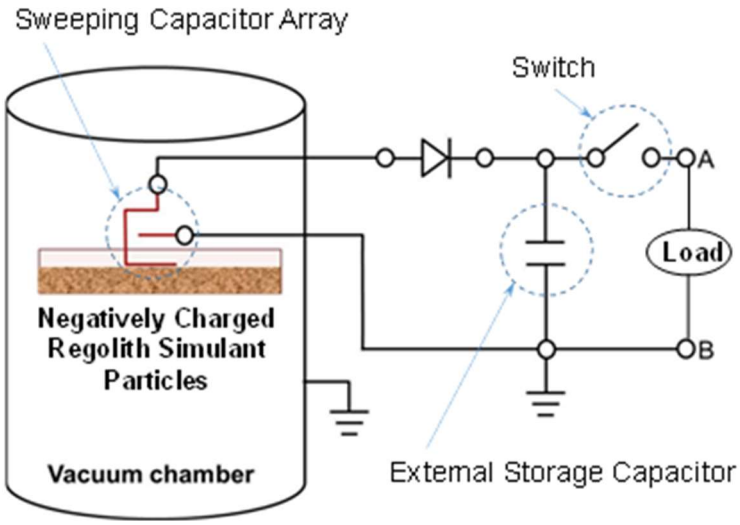

Figure 13. Schematic diagram of the experimental charge collection circuit.

Test Results: The regolith simulant was initially charged by the impinging electron-beam with a voltage at 25 keV and beam current of 0.728 mA. After the simulant was charged in vacuum by the electron beam for various selected exposure periods, the electron-beam was turned off and then a 390 pF capacitor was run over the simulant surface to collect the charges. Figure 14 shows the series of measured maximum charge voltages and collected number of electrons for the cases of electron charge period from 1 minute to 30 minutes by the flood e-beam source. It is very obvious that the longer the simulant is charged, the more the number of electrons is deposited and collectable. Two numbers on each peak shown in Figure 14 indicate the capacitor voltage (in black) and collected number of electrons (in red). On the x-axis of the plot in Figure 14, the time intervals indicate the decaying times by leakage current on each run-cycle of charge/discharge. The decay rate is mainly due to the leakage current from the edges all around the capacitor array we made at our laboratory. The side edges of capacitor array were not electrically sealed for insulation. Accordingly, much of the collected electrons quickly leaked out through the open edge of capacitor array. We anticipate that the optimized leak-proof design of capacitor array would show the charge stability with very slow decay rate.

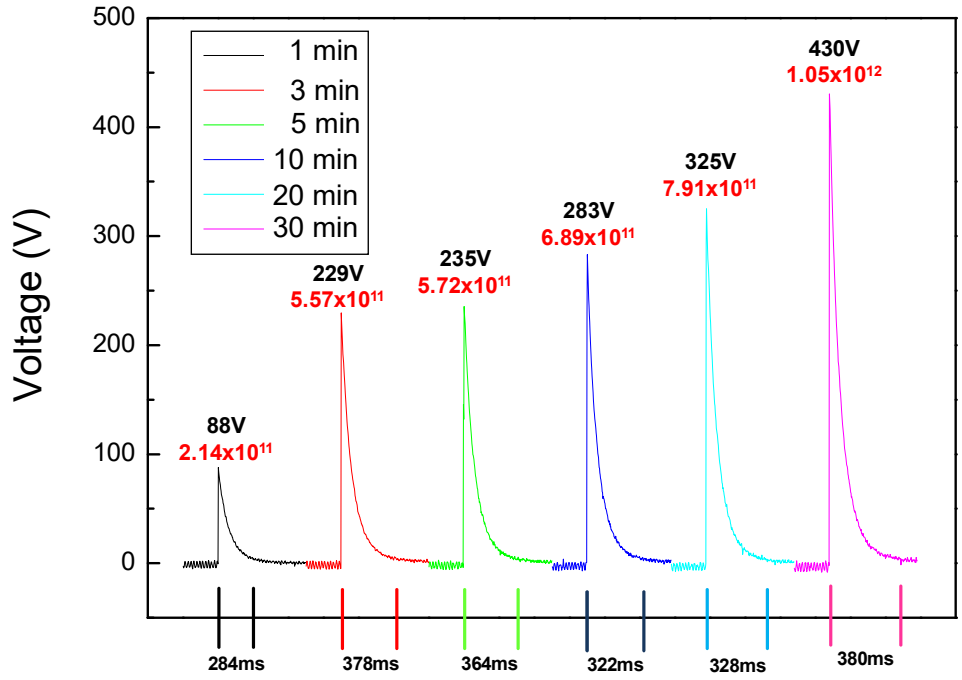

Figure 14. Measurements of charge and discharge with 390 pF single-plate capacitor based on the charging time from 1 minute through 30 minutes.

The charge collection rate is determined by the speed of the capacitor carriage and the contact area of simulant. When the lunar simulant was charged with the e-beam flux of 10 keV and 0.620 mA for 3 minutes, the capacitor array was then dragged over the soil with run time intervals of 3.25, 3.00, 2.96, 2.71, and 1.29 seconds, corresponding to velocities of 3.1, 4.5, 6.0, 7.3, and 8.7 cm/s, respectively. The measurement data of collected charge voltage and number of collected electrons based on the test parameters: E-beam source with 10 keV and 0.783 mA emission beam current; vacuum at 8.6 x 10^{-6} torr; E-beam illumination time of 3 minutes; carriage moving distance of 40.6 cm; and grain size of simulant of 367 nm, were plotted against the speeds of the charge collector in Figure 15. An expected linear trend of charge collection from 500 V to 300 V along with the speed of collector is shown by a dotted line in Figure 15. The charging voltages are dropped from about 500 V down to 430 V, 375 V, and 275 V, correspondingly, along with increasing the velocity from 3.1 cm/s to 4.5 cm/s, 6.0 cm/s, and 7.3 cm/s, respectively. The results show clearly that the faster the speed, the smaller the charge collection. However, actual measured data for charge collection based on selected speed shows rather a curvy nature. This is most likely due to the fact that the E-beam flux is not geometrically uniform over the area of exposure.

Mitigation of fine dust and electrostatic accumulation from lunar regolith had imposed serious problems, such as abrasiveness on bearing, pervasiveness as coating on seals, gaskets, and

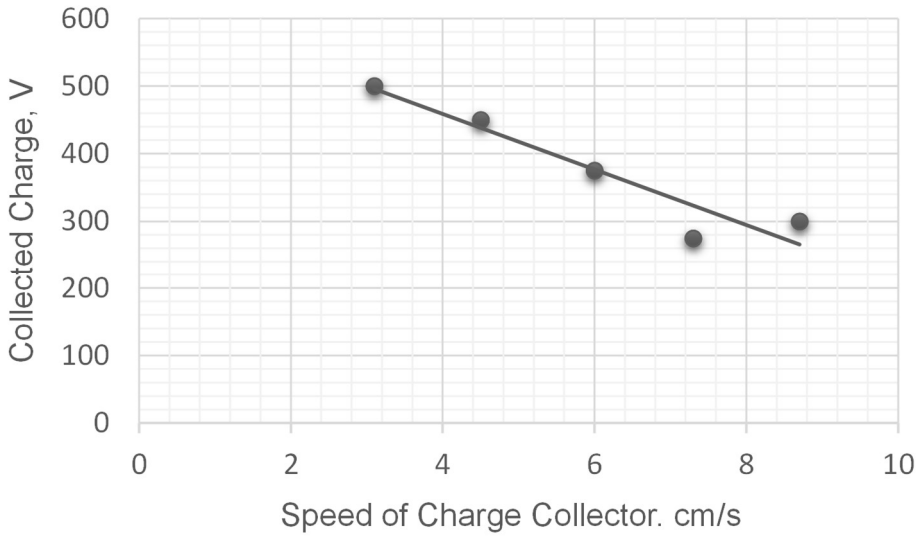

Figure 15. Measured charge/discharge rates vs. speed of capacitor array.

lenses, and physiological effects on astronauts and robotic systems for Lunar missions [61]. The basic mechanism of dust adherence is due to the electrostatic attraction of disturbed and levitated electrically charged dust. Removal of adhered dust is neither trivial nor readily doable.

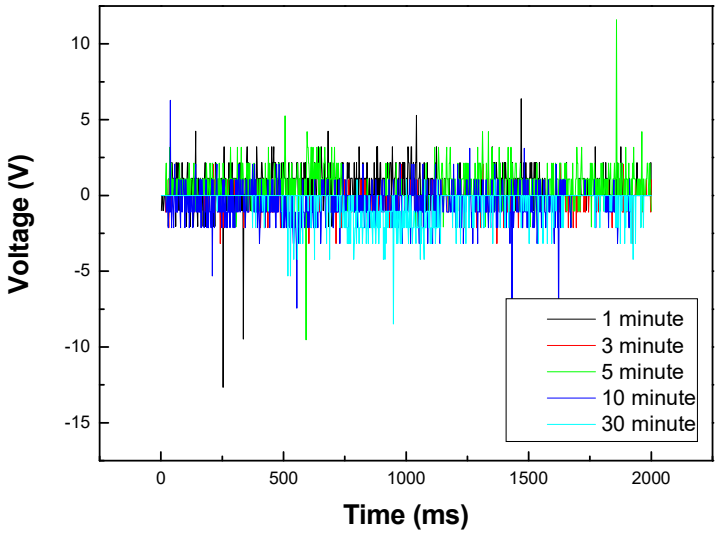

Figure 16. Measured data of charge collection during backward track.

One study shows a method of using an electrodynamic dust shield to repel the approaching dust particles by applying opposite charge to remove the already adhered dust by dielectrophoretic forces [62]. Brush removal of already adhered dust was reported but not effective [63]. Prevention of dust mitigation can be done by neutralization of charged particles. The experiment carried out for the ESPG development also gives a benefit of dust mitigation by charge neutralization. Figure 16 shows the measurement count of charge collected during the

backward track of capacitor array is almost negligible. Since the forward track has collected most of charges, the backward track does not have much charges to collect.

ESPG Application to Rover: Based on the experimental study discussed above, an array of capacitors was designed for rover application as shown in Figure 17 to collect the charge and at the same time to neutralize electrostatically charged regolith. In its final form, an array of single-layered, flat capacitors securely attached to a motorized lunar buggy would collect the charge

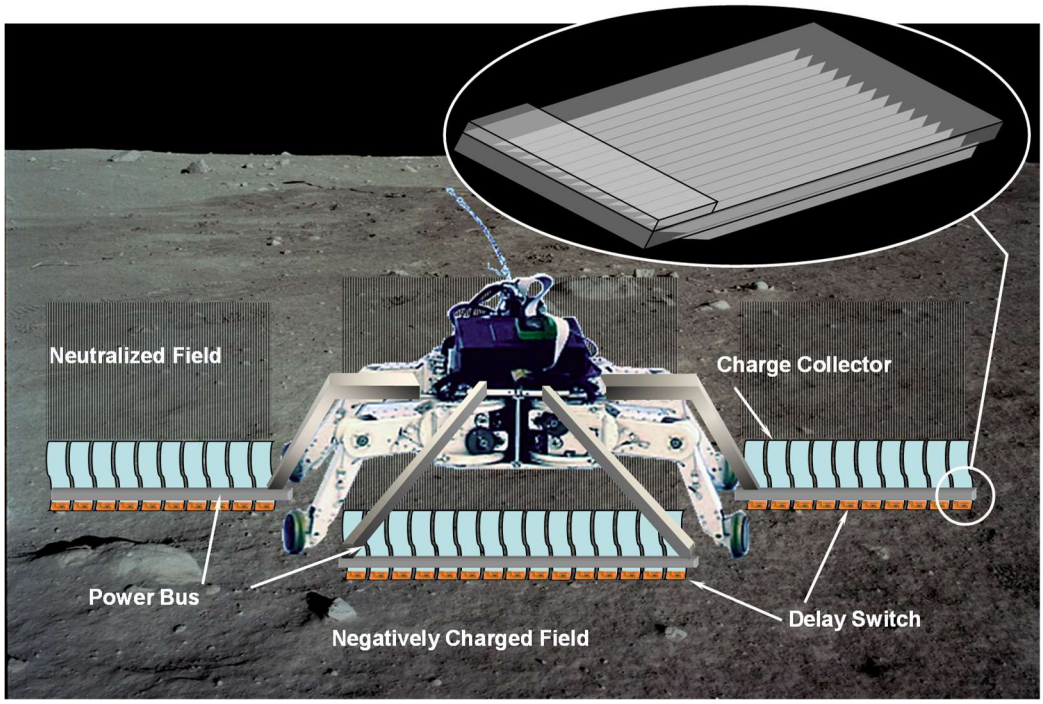

Figure 17. Lunar buggy with electrostatic power generation system.

from the lunar surface. The charge collector consists of a thin-film array of capacitors that are continuously charged and sequentially discharged using a time-differentiated trigger discharge circuit to produce a pulse train of discharge for DC mode output as shown Figures 18 and 19. An array of flexible capacitors, as previously shown in Figure 12, was designed to freely run over any rugged objects on the lunar surface. To optimize charge collection, metal-insulator-metal (MIM) capacitors can be fabricated with a physical vapor deposition process to control the thickness and maximize the capacitance. The capacitor strips also could be configured in an array with several electron capture blades that rake through the lunar soil. Several of these arrays can be linked together for wider coverage.

Figure 19 shows a circuit for electrostatic power generation that collects and converts capacitively charged electrons into modulated power with differential drain delay described by the equivalent circuit in Figures 18 and 19. The parameters determining the time delay are the electrical resistance (R), the inductance (L), the Gordon dispersivity (or confinement) factor (G), and the capacitance (C) at a given frequency (ω). This circuit consists of a variable DC-DC transformer, rectifier, smoothing capacitor, and regulator, and can be duplicated and combined with several other charge collection capacitors in order to generate a steady DC power output.

Studies made on the charge density of lunar soil predict about several thousand volts of electrostatic charge [45, 47]. One simulation study done at NASA Kennedy Space Center predicts the negatively charged lunar soil can reach a voltage of about 700 [49]. A report by T.

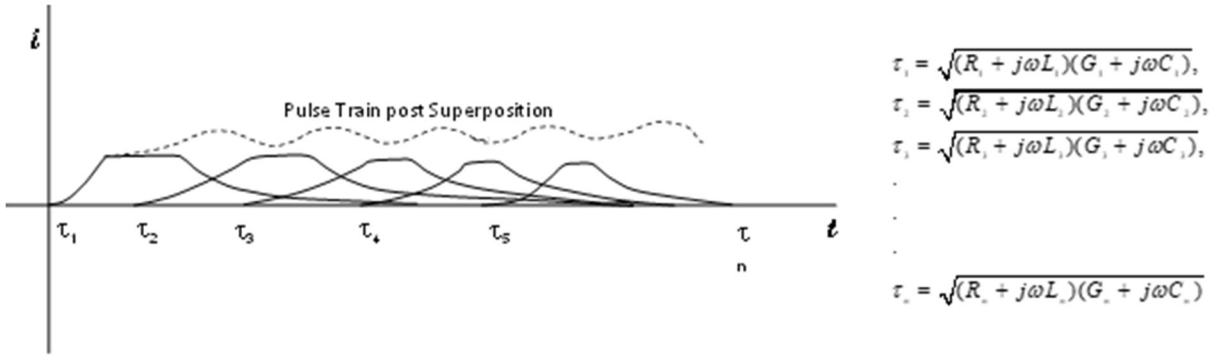

Figure 18. Pulse mode modulation by delay circuit.

J. Stubbs et al. [48] discusses triboelectric charging, a transfer of charge from the body to another as they contact each other. The estimate made by Stubbs et al. [48] is that approximately 10^5 electrons are gained through inter-grain contact by an individual grain of

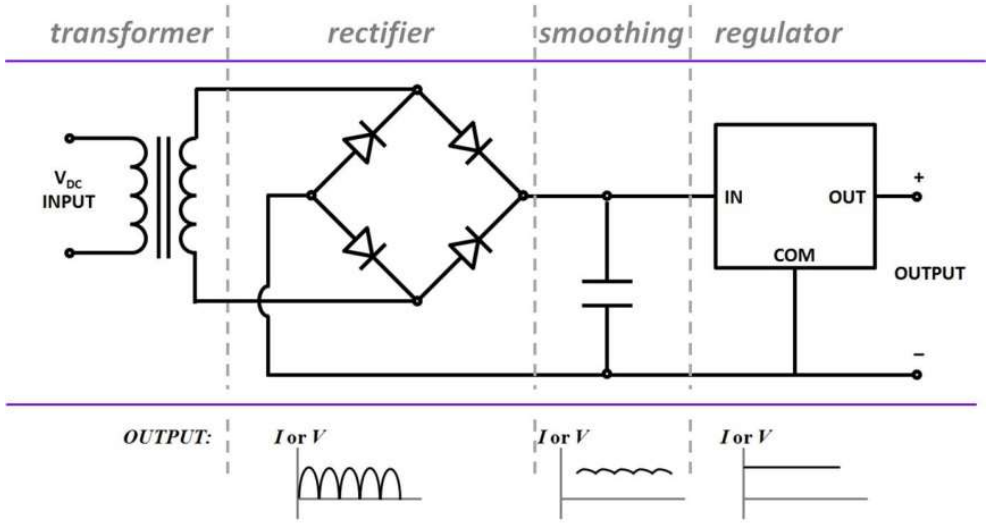

Figure 19. Regulated DC power generation circuit.

lunar soil (diameter ≈ 50 μm). For a 10-blade collector, with each blade 5 cm high and 30 cm long (2 collection sides = 300 cm^2), the charge accumulation can be estimated using the contact area of blades. For the purpose of a design study on a charge collector that will run on the lunar surface, it was assumed that a lunar dust grain has been charged and accumulated approximately 10^7 electrons over 4 billion years of exposure. The charge collector, with 10 blades plus array base, would have a total contact area of about 3300 cm^2 and would contact 132×10^6 grains (maximum) of lunar soil. In this case, the total maximum charge transfer at any

given moment would be 132×10^{15} electrons, corresponding to a charge of 21×10^{-3} C/s or 21 mA for a 10-unit array moving at 30 cm/s.

Utilizing an open circuit voltage of 700 V [36], the total maximum theoretical power which can be harnessed from the lunar soil would be 5.88 W per array. The parameters used for the

Table 3. Parameters used for estimating charge collection by Lunar buggy electrostatic power generator.

Parameters	Estimated Values	References / Notes
Negative Charge	- 700 volts	[ref. 1]
Grain size of lunar soil	~ 50 μm	[ref. 33]
Triboelectric Charge	~ 10^5 electrons	[ref. 52]
Solar-Electron Charge	~ 10^7 electrons ~ 1.602 x 10^{-12} Coulomb	[ref. 30] by exposure from solar plasma
Charge accumulated	~ 10^7 electrons	On each regolith particle
Size of Collector Blades	5 cm x 30 cm x 2 each	Design value
Charge Transfer Area	300 cm^2	Both sides of a single blade
Area for 10 blades	3000 cm^2	Area of 10 blades
Train Base Area	10 cm x 30 cm	Base structure for 10 blades
Train Base + 10 Blades	3300 cm^2	Charge interfacing unit area
# of Contacting Grains	132 x 10^6	3300 cm^2/ $(50\ \mu m)^2$
Total Charge Transfer	132 x 10^{13}	$132x10^6 \times 10^7$ electrons
Collector Motion	30 cm/sec (refresh/sec)	Speed of rover
Total Charge Rate/unit	0.00021 Coulomb/sec	0.21 mA/unit
Unit # per bus array	10	Each bus formed by 10 units
# of Buses	4	Rover drives with 4 buses
Total Charge Rate/4 arrays	8.4 mC/sec	8.4 mA
Power Collection/array	5.88 Watts (=8.4 mA x 700V)	at 700 volts charging voltage

estimation of ESP module performance are listed in the Table 3. The results from this estimation are tabulated in Table 4 to compare with high efficiency multi-junction photovoltaic cells. From the results in Table 4, there are some advantages of ESP modules as compared to the multi-junction solar cells. The power collected by the ESP module appears very attractive since it can be also used during the approximately two weeks of lunar nights where sun light is not available. The fabrication of ESP modules is fairly inexpensive as compared to the multi-

junction solar cells. The only drawback of ESP modules is a short life expectancy since the ESP modules are being dragged on the lunar soil surface. A short useful life of ESP modules can be compensated by replacing the damaged ones with spare modules. The damaged modules can be readily replaced mechanically with spare modules. The ESP module is very light weight due to its thin-film structure that allows for several of them to be carried as spare parts for replacement.

Table 4. Performance comparison between electrostatic power generator (ESPG) and photovoltaic (PV) cell.

	PV Cells	ESP	Notes
Device Concept	Boeing's Spectro Lab Multi-junction	NASA LaRC's ESP Module	
Energy Source	Solar	Negatively charged Regolith	
Unit Area	10 cm x 30 cm	10 cm x 30 cm	
Incident Energy	40 watts	14.7 watts*	*Both Lunar day and night operation
Efficiency	40 %	90 %*	*Efficiency of circuit is much higher (>90%)
Collected Power	**16 watts**	**5.88 watts**	
Operation under	Lunar day only	Lunar day and night	
Energy Storage for Kick-off Power	No	Yes, for kick-off start	
Dust Mitigation	No	Yes	
Fabrication	Complex CMOS skill required	Fairly easy	In-house Fab

Based on the parameters tabulated in Table 3, a theoretical estimation of power collection was made with the rover-based ESPG concept shown in Fig. 17. The estimated result of ESPG was compared with the equivalent size of high-performance solar cell panel. If the parameters used for estimation are validly sustained for ESPG application, the power collected by ESPG will be 5.88W which is nearly comparable to that of ordinary solar cells with 17% efficiency. This comparison is tabulated in Table 4.

III. ARCHITECTURES OF MULTI-PURPOSE SOLAR CONCENTRATORS

We have witnessed the epochal progresses in conjunction with telecommunications and space technology that have nurtured and improved our civilization in our lifetime. The advancement in rocket propulsion, guidance, and orbital mechanics has allowed space exploration, spaceborne global communications, weather observation, security monitoring, resources management etc.

III-1. Review of Historically Significant Spaceborne Antenna and Telescope Technologies

Since early 1960, new structural concepts for spaceborne antennas and telescopes have appeared to provide satellite-based global communication and deep space exploration, respectively. Table 5 shows a summary of historical space structures.

Table 5. Space antenna structures

Structures	Year	Diameter, m	Shape/Precision	Materials	Who	Refs
Echo I Echo II	1960 1964	31 41	Inflated Sphere	membrane	NASA	[64]
OCDS	1970	100	parabolic	metal wire mesh	Grumann	[65]
LMSC ATS-6	1980s	55	parabolic	metal wire mesh	NASA	[66]
IAE	1989	14	parabolic	membrane	L'Garde NASA	[67]
ACTS reflector	1993	2.2~3.3	Parabolic/70μm	composite/graphite	NASA	[68]
Dornier reflector	1988	8	Parabolic/8μm	carbon fiber reinforced plastic		[69]
NGST	1997	10	Parabolic/75μm	graphite-epoxy	NASA	[70]

In Table 5, OCDS is a space deployable antenna concept to be assembled in space but never implemented. Throughout the following years, the need for new capabilities was always on the horizon, whether it was the desire for a system that was larger, cheaper, lighter, more durable, or more precise. In response to the demands of new capabilities, NASA has always led such technical challenges as history has manifested. For human space exploration, the Moon is

regarded as the first leg of colonization that requires many technical essences for the development of habitats, observatories, resources mining, and communication posts.

III-2. Cassegrain Concentrator:

To provide a sufficient solar power for regolith sintering process and other applications, several kinds of concentrators are considered: (1) Cassegrain system, (2) Segmented Cassegrain system, (3) Bi-segmented Cassegrain system, and (4) Fresnel lens.

Figure 20 shows the cross section views of front and side for a Cassegrain concentrator. The primary mirror has a parabolic shape and can be built with inflatable membrane materials or foam structure with low CTE and low Poisson ratio. For this Cassegrain system to be multi-functional, the primary mirror is an essential component and must be able to maintain optical grade precision requirements under the constraints of weight and volume. The frames of system

can be made with light-weight composite materials. However, since the primary mirror requires optical precision with near-zero optical aberration to maintain the resolution greater than λ/30, the selection process of materials for the primary mirror should consider the following parameters: low CTE, low Poisson ratio, lightweight, strength, suitability of reflective coating, and UV-resisted long life. The discussion of material selection for primary mirror will be discussed at Section IV.

The primary mirror can be swiveled by the motor to trace, align with and receive the sun light perpendicularly through the aperture. This function is offered by the sun-angle track controller. This track control function by an electrical motor is very important for not only solar sintering and harvesting gaseous molecules, but also setting space antenna and telescope to line up with targeted direction and search the target precisely.

The beam of light collected by the primary mirror is concentrated and directed to the secondary

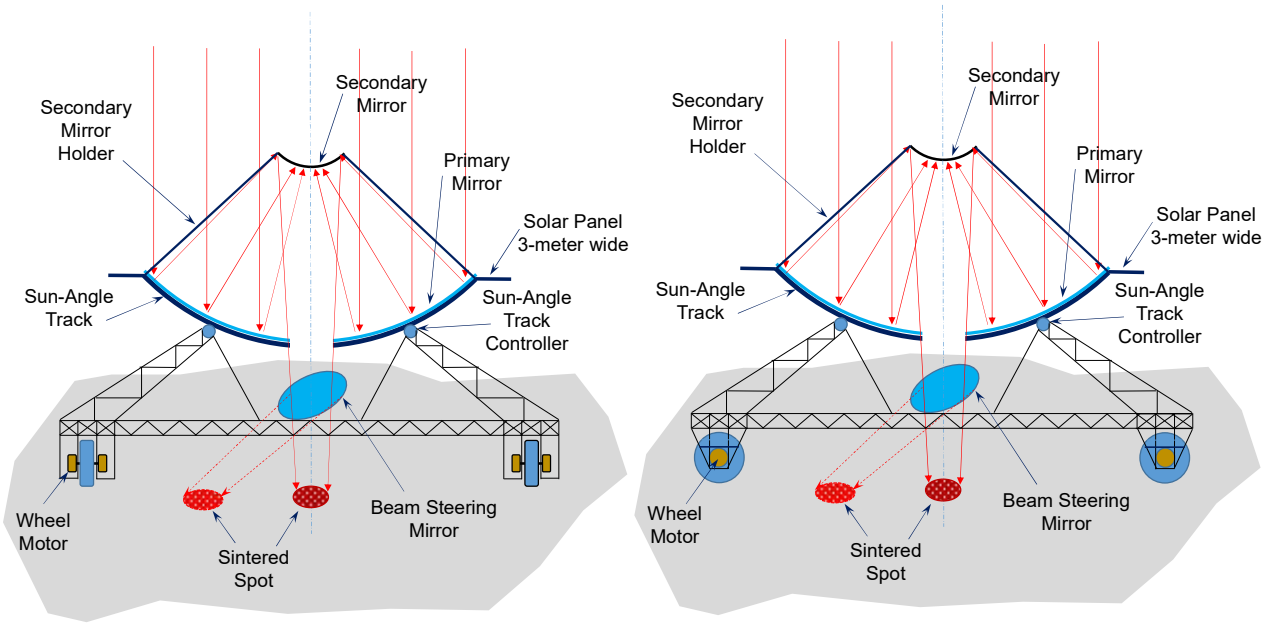

Figure 20. Front and side views of Cassegrain solar concentrator with power-wheeled substructure.

mirror where the concentrated beam of light is directed down to the beam steering mirror for solar sintering purpose, as shown in Figure 19. Otherwise, for the case of space antenna applications, the beam steering mirror is replaced by the injection horn/receiver antenna. For the case of space telescope, the beam steering mirror is replaced by an image sensor array to capture the spectral signals from an object. In the design process of this beam steering mirror platform, a turret system that is integrated with three components of the beam steering mirror, the injection horn/antenna, and the image sensor array together is desirable to offer the option of operation by rotating itself whenever the job is changed for any designated job.

The substructure of the Cassegrain system has several power-driven wheels to mobilize the system to follow the action scenarios. The power for driving comes from the solar cell array populated around the rim of primary mirror. The solar cell array of 29 % efficiency (i.e. multi-junction PV cell) is laid on a 3-meter wide surface extended from the edge of primary mirror

aperture. This size of solar panel provides a power greater than 100 kW. In case more power is needed, the panel width can be increased to generate more power. If it is 5-meter wide, the power output is going to be roughly 200 kW level. The power required for mobilizing the system shown in Figure 20 can be determined by the weight of the system, speed of motion, and operational range.

III-3. Segmented parabola reflector:

Figure 21 shows a segmented parabola reflector. Figure 21 shows a mono-segmented parabola reflector with the pivoted deflector that directs the focused sunlight to a single spot on regolith. This kind of reflector can also serve for sintering, harvesting gaseous molecules, and space antenna only.

III-4. Bi-Segmented parabola reflectors:

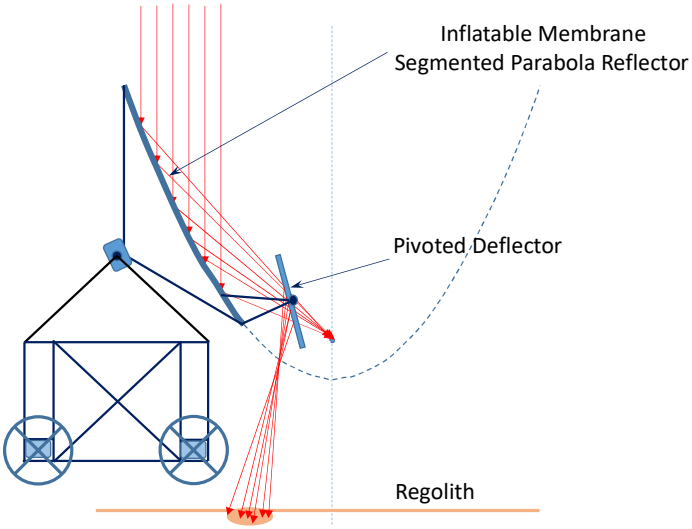

Figure 21. Segmented parabola solar concentrator

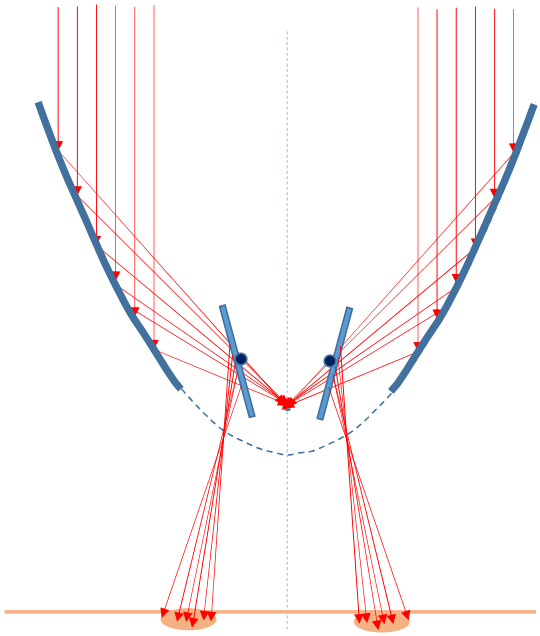

Figure 22. Bi-segmented parabola solar concentrator

Figure 22 shows a bi-segmented parabola reflector that draws two focused spots on regolith. These two concentrators have structurally formed with one or two segments. The bi-segmented parabola has wider receiving area of solar flux. If we consider space antenna application of the bi-segmented, it can beneficially offer the capability of dual beam signal handling as a space antenna.

III-5. Fresnel lens:

Figure 23 shows an array of the Fresnel lens. A large size of Fresnel lens can be fabricated by densely populating the number of ring gratings fabricated on transparent plane structures. Multiple Fresnel lens with beam deflector can be combined and used to illuminate regolith with a

sufficient solar power as shown in Figure 23. The Fresnel lens has only a single role for solar sintering.

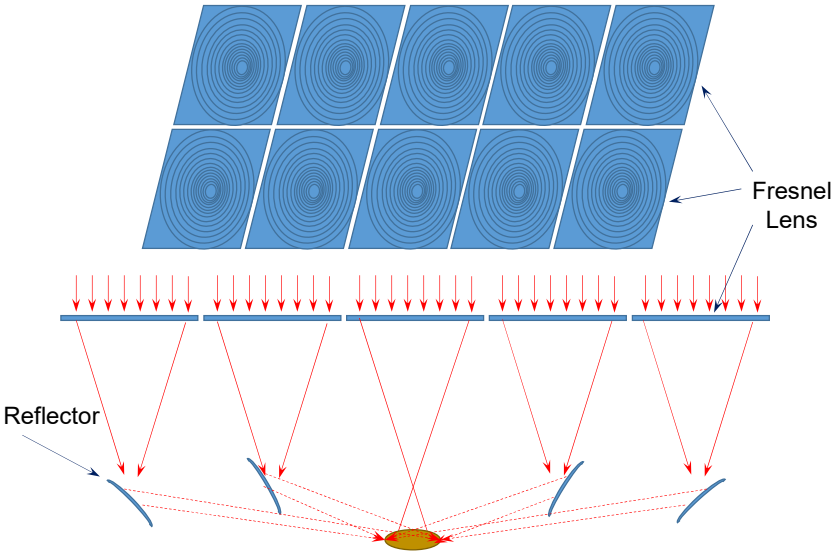

Figure 23. Array of Fresnel lenses with reflectors

III-6. Assembly of Cassegrain system:

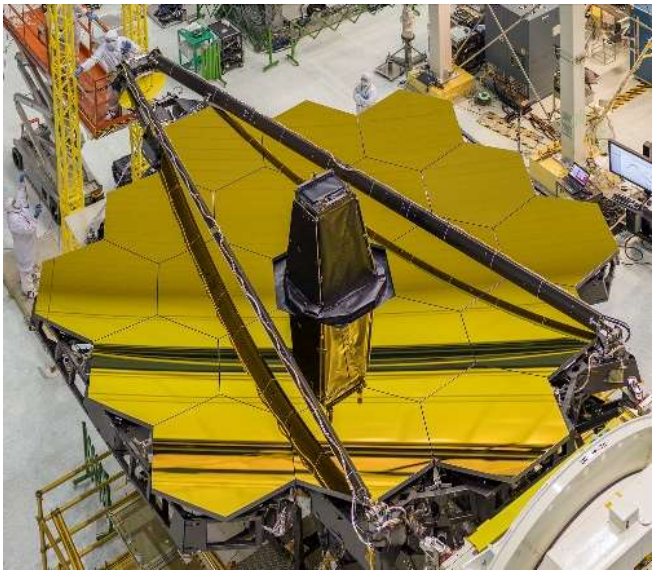

Figure 24. James Webb Space Telescope. (Credit: NASA)

A large size of reflectors shown in Figures 20, 21, 22, and 23 can be fabricated with modularized segments that may be made out of flexible membrane materials. In such a manner, the transportation of the compacted modules to the Moon is feasible. For a segmented optical mirror, the feasibility of onsite assembly must be exercised before deployment, just like the hexagonally segmented mirrors of James Webb Space Telescope (JWST) (Figure 24). The onsite assembly of solar concentrators is going to be a tough challenge to work under hostile environment, but still much better than unattended onsite assembly of JWST-like structures. Having the features with onsite self-assembly capability seems very attractive and important, but technically it is hard to implement onsite self-assembly. One possible scenario is a combination of capabilities for onsite assembly and self-assembly. Some of the sub-structures can be pre-assembled before launch. Some of the structures can have self-assembly features. Onsite, these substructures are fully assembled into a functional entity by the assisting interventions of astronauts.

IV. APPLICATIONS OF MULTI-FUNCTIONAL CONCENTRATOR TECHNOLOGY

The purpose of this study is to illustrate a better and large-scale concentrator design with new lightweight materials that warrant a low CTE and negligible Poisson ratio. NASA Langley has a very talented team in materials technology who has dedicated to develop lightweight functional materials, such as foams and composites, throughout the last several decades for NASA missions. This team is able to develop new materials qualified for large-scale primary mirror that yield far better a single embodied structure or segmented structures in place while also performing other mission capabilities relevant to lunar and science missions on or from the lunar surface. Several candidate materials for large-scale primary mirrors will be discussed in later sections.

IV-1. Solar Sintering

Thermal energy required for regolith sintering is calculated using the aperture diameter of a concentrator and the thermal properties of lunar regolith simulant. Considering the 90 % reflectivity of solar flux by the primary and secondary mirrors of Cassegrain system, the combined loss is 19% and the majority (81 %) of solar flux can be concentrated on regolith for sintering. For the multi-purpose use of Cassegrain system, especially as a space telescope, the optical reflectivity would be much higher than 90 %. However, only 75 % of the total incident solar energy on regolith surface, instead of 81 %, was used for the solar sintering calculation. Therefore, the use of 75 % solar flux in the calculation is a reasonable estimation. For sintering alone, the arc-minute level deviation in the angle of incidence through the aperture of concentrator is not significant because the sintering area is wide and what matters most is the effective solar thermal loading into the regolith.

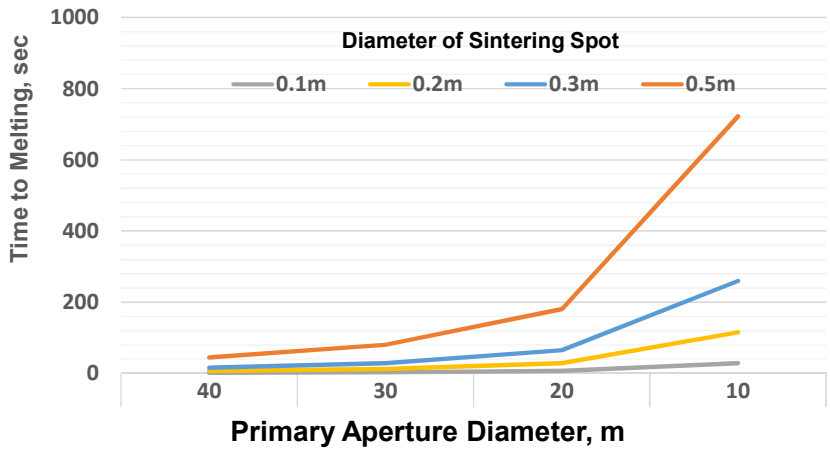

Figure 25. Sintering time to sinter 8 cm of regolith based on solar concentrator size and sintering area.

Thermal properties of regolith used for the calculations were obtained for a regolith simulant but are close to the actual properties of lunar regolith. The values of these thermal properties used are the specific heat: 1.63 kJ/kgK [71], the melting points: 1373 ~ 1653 K [72], and the density: 1.5 g/cm^3 or 1500 kg/m^3 [73].

Using these parameters, the time to sinter the regolith up to 8 cm thick by a single rasterizing pass of focused solar flux was estimated. With several respective spot diameter sizes of focal area, 0.1 m, 0.2 m, 0.3 m, and 0.5 m, the melting times required for 8 cm thick regolith are plotted in Figure 25. The solar concentrator's aperture diameters are shown on the X-axis. The table listed below the X-axis of Figure 25 shows the melting time in second of regolith based on

the diameter of melting spot under the solar concentration. Table 6 lists the calculated results of melting times in second while sintering an 8 cm thick regolith according to the focal plane spot size and the solar flux collected by various size of concentrator apertures. For example, to sinter 8 cm thick regolith using the focal area of 50 cm in diameter, it takes 45 seconds with a Cassegrain concentrator with 40-meter aperture diameter, 80 seconds with 30-meter aperture,181 seconds with 20-meter aperture, and 723 seconds with 10-meter aperture.

Based on the theoretical estimation tabulated on Table 6, the time to sinter a 30 meter diameters of landing pad is listed at the last row of Table 6. Figure 26 shows a multilayer sintering scheme to make a thick and hardened pad. If the first layer of hardened sintered bed is not thick and strong enough to hold the weight of landing rocket, then additional layers can be built on top of each other as multiple layers to sustain the weight of landing rocket. To develop multiple layers of sintered regolith, regolith is evenly spread over the top of the previously sintered layer to a certain thickness. Then a concentrator runs over this newly spread regolith to sinter to the first layer. The thickness of regolith spread and sintering time can be adjusted to build a firm and strong embodiment of added layer with the layer below. Such a sintering process can be used for multiple over-coating over the habitats with sintered regolith layer that works for radiation shielding.

Table 6. Sintering time based on diameters of solar concentrator aperture and melting spot.

Thickness of Regolith 8 cm		Primary Aperture Diameter			
		10 m	20 m	30 m	40 m
Diameter of Sintering Spot	0.1 m	29 sec	7 sec	3 sec	2 sec
	0.2 m	116 sec	29 sec	13 sec	7 sec
	0.3 m	260 sec	65 sec	29 sec	16 sec
	0.5 m	723 sec	181 sec	80 sec	45 sec
Landing Pad	30 m diameter	2008 hrs	502 hrs	223 hrs	125 hrs

IV-2. Collection of Gaseous Molecules:

Regolith Trapped Gaseous Molecules: The total solar power collected by a 20-meter concentrator would be approximately 400 kW. This 400 kW is a combination of multi-spectral photons with photon energy roughly varying from 0.1 eV to 6 eV that can easily detach and remove molecules, such as H_2O, He-3, and/or other gaseous molecules that are dangling to regolith particles rather than chemically bonded compounds. The photon energy is sufficiently high enough to easily break down the dangling bonds of gaseous molecules. With solar concentration, the increased number of photons that interact with molecules increase the breakdown probability of dangling bonds by the photon collision (or coupling) frequency (with high flux density of spectral lines) and subsequently by thermal effects too. Intensity of solar photons (0.1 eV ~ 6 eV, here 1 eV is equivalent to 11,600^{o}K) is not high, but the concentrated

solar flux increases the number of photons that can be incident on and coupled with gaseous molecules. If anyone counts thermal effect only for detaching gaseous molecules in their estimation, they will find that thermal energy is required much more than necessary for breaking down of dangling bond of these molecules, since in this case thermal energy is consumed to heat up not only these molecules, but also the regolith particles which are much more massive than these molecules. Heating up of regolith takes more energy due to its large thermal mass.

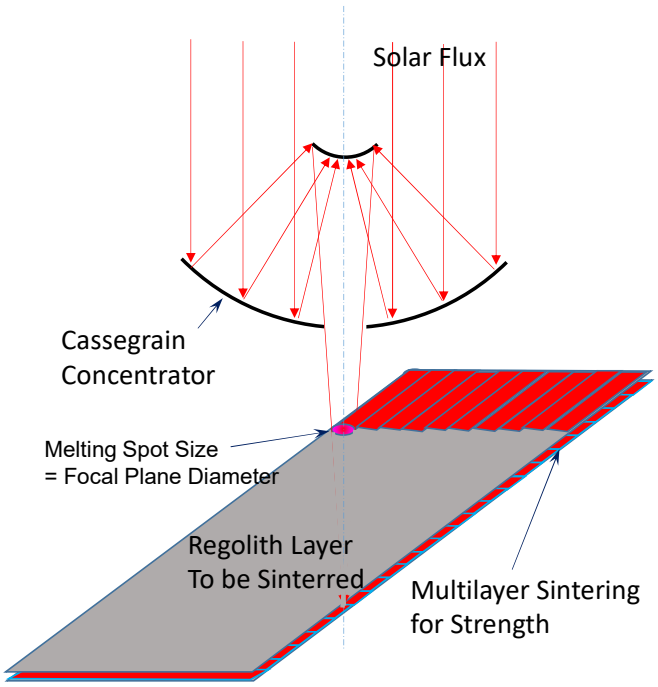

Figure 26. Multilayer sintering scheme.

The collection of detached molecules from regolith is not easy to fulfill since the environment on Moon is quite harsher than anticipated. It is virtually vacuum (10^{-12} torr), no atmospheric pressure and low gravity (1.62 m/s^2). Any molecules released will have free translational linear motions in all directions because of low collision probability that means no Brownian motion. The number of released molecules from regolith by solar thermal heating is also very few and scattered out to all directions. Therefore, it is very hard to guide them to a direction for collection, even using the conventional pressure differential. Accordingly, a new approach is necessary to capture and store the released gaseous molecules.

The environments on the Moon and Mars may not allow use of those equipment developed for terrestrial applications. Specifically, the harvesting of gases, such as He-3, H_2, O_2, and water vapor, is not easy on the Moon-like environment of near vacuum (10^{-12} torr). It is important to

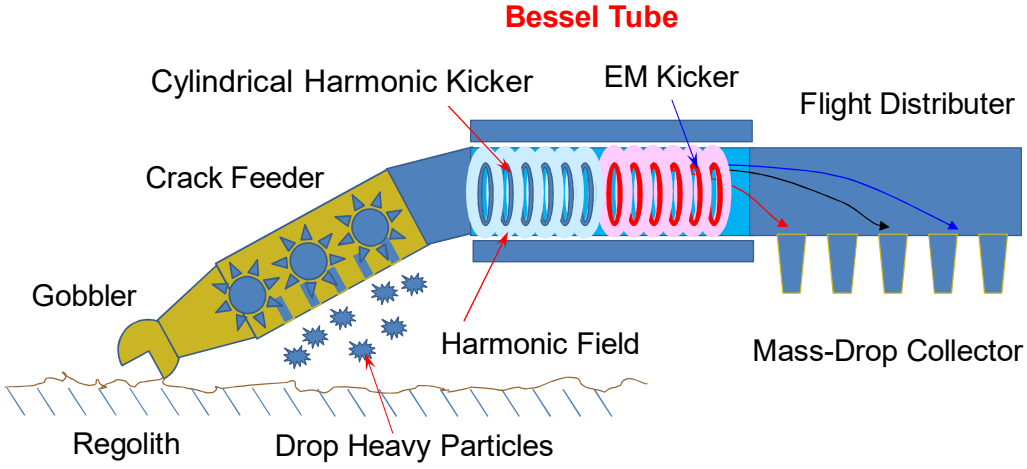

Figure 27. Overall concept of Bessel Tube for harvesting volatile elements. [74]

have onsite supply capability of valuable gases, such as He-3, H_2, O_2, and water vapor during lunar and Mars explorations for synthesis of propellants and O_2 and H_2O for habitats. New technology developed at NASA Langley specifically for harvesting gases on the Moon is called 'Bessel Tube', as shown in Figure 27, which is based on the principle of cylindrical harmonic generator. This equipment captures and accelerates gaseous elements through the drift axis of ring-field equipotential domain. The accelerated gaseous elements are eventually stored selectively into a bottle by induction field at the other end. Figure 27 shows the concept of the Bessel Tube [74] for harvesting volatile elements from regolith.

The proposed Bessel Tube is a new and innovative concept and technology to capture and

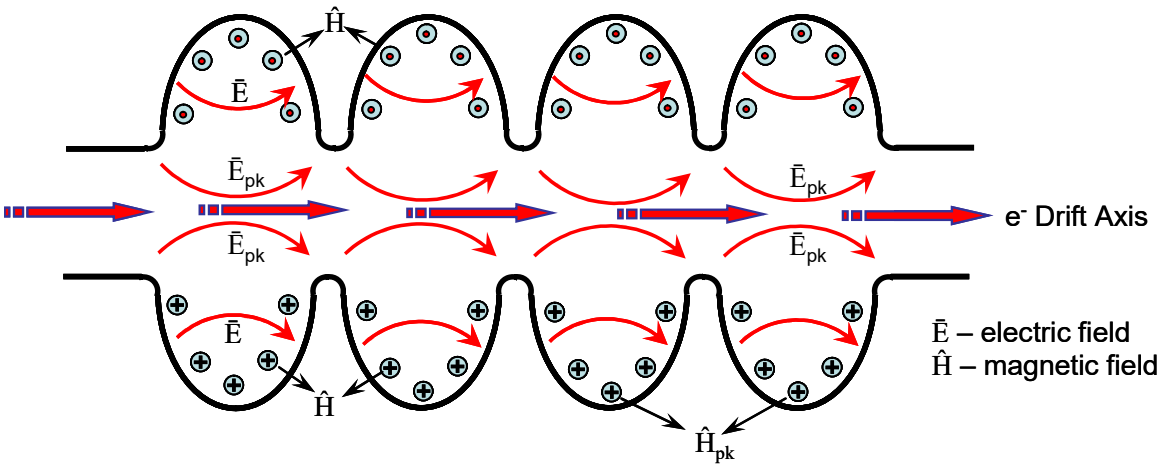

Figure 28. Cylindrical harmonic generator in a hypocycloidal mode for accelerating electrons.

accelerate gaseous particles through drift axis using circularly harmonic field or ring-field generator. However, the laboratory and theoretical approaches to elucidate the phenomenon of drift velocity of gases have not yet been fully exploited to a level beyond postulation. Circularly harmonic fields, in principle, establish the cylindrical harmonic condition on the basis of axi-symmetric electric polar arrangement. A typical example of the axi-symmetric electric polar arrangement is the arm-chair style of carbon nanotubes (CNT) with zero chirality which theoretically exhibit a ballistic transport property of electrons. The principle of nano-scale electron drift channel is clearly well-defined by the theory of mesoscopic conductor [75]. Another example can be seen from the electron acceleration concept along the drift axis where the equipotential of E-field develops a cylindrical harmonic in a hypocycloidal mode as shown in Fig. 28. The helicity of a particle is defined as the projection of a spin vector $\vec{s}$ in the direction of its momentum vector $\vec{p}$, as $\vec{h} = \frac{\vec{s} \cdot \vec{p}}{|\vec{s} \cdot \vec{p}|}$. Therefore, if a particle's spin vector points in the same direction as the momentum vector, the helicity is positive, and if they point in opposite directions, the helicity is negative. However, the helicity of a massless particle is always equal to its chirality. The helicity of a particle is a Lorentz invariant. A helical structure of polar elements creates a scattering mode in which the static field pattern of helically arranged field elements within the helical tube deviates the vector field of motion. If the helicity of ring field is zero, it will appear to be hypocycloidal as described in Figure 28. Suppose that the helical tube is axially

symmetric and uniform in diameter and has no helicity. The hypocycloidal fields (HCF) from the polar elements (i.e. E-field) of helical tube eventually develop equipotential field lines along the center axis of a tube. The hypocycloidal dips are actually filled up by the superposed fields. Hence, the HCF is relaxed to be a pseudo linear field (even if a minute helicity exists) along the axial direction, thus forming a cylindrical harmonic (CH) condition. Such a CH condition warrants the ballistic transport of electrons, charged particles, or particles with dipole moment through the axially symmetric drift channel. Such a phenomenon is enabled by the existence of cylindrical harmonic if the helicity of polar field is negligible. Accordingly, the technical aspect shown in Figure 27 will drive particles with dipole moment, such as He-3 and H_2O through the drift axis in Bessel Tube. The CH condition may not be suitable for hydrogen and oxygen molecules, unless these molecules are ionized. Hydrogen and oxygen molecules are regarded as homonuclear (nonpolar) molecule without electronegativity difference between H-H and O-O bindings. That's why these molecules need to be ionized for the Bessel tube. These molecules can be easily ionized by the electron beam or vacuum UV. Then these molecular ions can be easily driven by the cylindrical harmonic field.

A cylindrical harmonic generator with E-field can be fabricated and tested to accelerate gases through the drift axis. The ring field formation in a linear array forms a field pattern of cylindrical harmonic and hypocycloidal mode that will drive gases with a dipole moment through the drift axis of Bessel tube. The gas molecules, driven by the gradient field formed by a series of ring-fields in a serial mode along with the axial center, pass through a region where quadruple poles deviate or deflect the momentum of a molecule and cause a specific molecule to drop at a specific location based on the magnitude of momentum. Like the particles in a mass spectrometer, a mixture of different molecules is separated into individual particle groups based on their mass through quadruple poles (EM kicker shown in Figure 27). A molecule with high mass flies a further distance than the one with light mass does. By this separation scheme, individual gas species are separately collected and stored in each container.

The production of gaseous molecules by solar sintering technology together with Bessel tube offers an added value to the scenario of solar sintering process. Collected gas molecules are very valuable and useful resources to enable propellant production and water supply required for space mission. Since the atmosphere of the Moon is very scant and almost vacuum (10^{-12} torr), there may be no possibility to harvest any gaseous molecules from the lunar atmosphere.

However, there might be a measurable amount of trapped gaseous molecules in regolith due to the fact that the stream of electrons, protons, and helium from solar flares interacts with lunar soil, mostly oxides, and splits oxides to generate oxygen atoms (see Figure 1). These oxygen atoms can be coupled with proton to form hydroxyl (OH) and water molecules. Recently it is known that hydrogen atoms and molecules, or even OH/H_2O are wide spread over the lunar surface [76].

Harvesting Helium-3: A study, based on the lunar regolith samples collected through Apollo-(11~17) missions, reveals that the lunar soil regolith reserves roughly over 2 million tons of helium-3 (He-3) [77]. It is well-known that He-3 is the only stable isotope of any element with more protons than neutrons. As listed in Table 7, the nuclear fusion of He-3 + He-3 releases large amount of energy without emitting neutrons. However, the fusion of He-3 atoms requires very high temperature that is much higher than in other fusion reactions. Neutron absorption

causes materials to become radioactive and to undergo nucleogenic or radiogenic processes. However, Helium-3 is known to be a fuel for aneutronic nuclear fusion for both reactions of deuterium and He-3: 18.3 MeV and He-3 atoms: 26.2 MeV, as shown in Table 7. The fact that aneutronic fusion process of He-3 enables extracting large amount of energy is very attractive for most of space fairing nations. These nations who have expressed their interests in mining He-3 [78, 79] as a part of their lunar exploration are Russia, China, India, and Japan. He-3 also

Table 7. Nuclear fusion reactions and Helium-3

Fusion Reactions Involving Helium-3			
Reactants		Products	Output Energy, Q
1st Generation Fuels			
$^{2}_{1}H + ^{2}_{1}H$	→	$^{3}_{2}He + ^{1}_{0}n$	3.268 MeV
$^{2}_{1}H + ^{2}_{1}H$	→	$^{3}_{1}H + ^{1}_{1}p$	4.032 MeV
$^{2}_{1}H + ^{3}_{1}H$	→	$^{4}_{2}He + ^{1}_{0}n$	17.571 MeV
2nd Generation Fuels			
$^{2}_{1}H + ^{3}_{2}He$	→	$^{4}_{2}He + ^{1}_{1}p$	18.354 MeV
3rd Generation Fuels			
$^{3}_{2}He + ^{3}_{2}He$	→	$^{4}_{2}He + 2\ ^{1}_{1}p$	26.200 MeV

has a whole variety of other applications than as a fusion fuel, such as homeland security, national security, medicine, industry, and science. For example, He-3 is used for neutron detection by measuring the scintillation emission when high pressure He-3 absorbs neutrons. By the increased demands, currently the stockpile of He-3 has been dwindled drastically to roughly 50,000 liters by 2010 after when the production of He-3 was outpaced by the increased demand from 2001. Additionally, to create more challenges, the projected He-3 demand in FY18 alone (100,000 liters) already exceeds the current stockpile and supply together [80, 81]. It was predicted that He-3 is going to be an expensive item that will exceed $3bn/ton [82]. It is known that the Moon has over a million tons of He-3. The harvest of He-3 is a challenging venture that requires a huge amount of commitment in resources and scientific wisdom. When the solar sintering process is used on the Moon, the side benefit of the mission is the harvesting of He-3.

Bessel Tube as a Sniff Atmospheric Sensor: The gaseous planets with thick and dense atmosphere in our solar system are Venus, Jupiter, Saturn, Uranus, and Neptune. Even some moons of these planets are known to have atmospheres. Titan, the largest moon of Saturn, is the only moon known to have a dense atmosphere. Since Titan shows a clear evidence of stable bodies of surface liquid and water ice, it is possible to postulate any bio-activity on Titan by even analyzing the constituent gas species of Titan at a close proximity through a fly-by. The current gas species data of Titan's atmosphere was identified by spectrometers onboard Voyager I and Cassini spacecraft. Titan's atmosphere is composed of nitrogen (97 %), methane (2.7 %) hydrogen (0.2 %) and trace amounts of other gases [83]. The measurement of gas

species in these gas planets and moons can be easily done by an onboard Bessel tube sensor of fly-by spacecraft. The Bessel tube for this purpose can be slightly modified from the

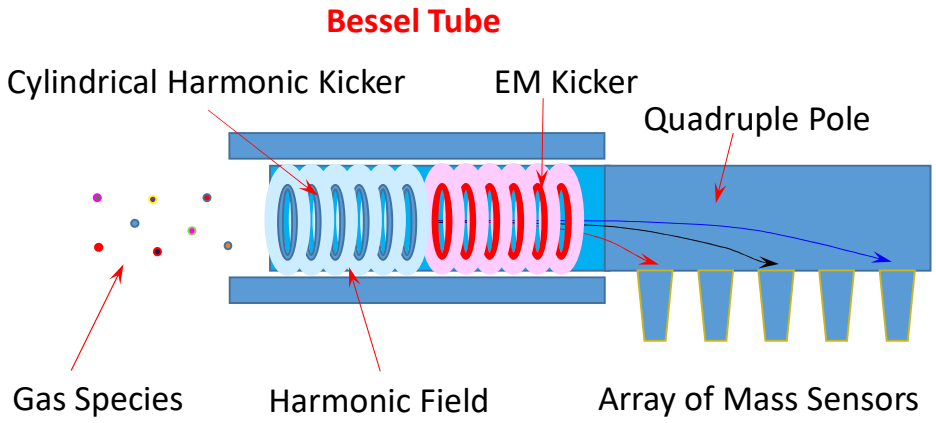

Figure 29. Bessel tube concept as a sniff atmospheric sensor for measurement of constituent species of Titan and gas Giant planet atmospheres.

configuration appeared in Figure 28 by simply removing the front end of the system, such as the gobbler and crack-feeder. Figure 29 shows a Bessel tube miniaturized to a finger size.

IV-3. Radiation and Meteoroid Protection Layer

After the solar concentrator is used to build a landing pad, it can be continuously used to make construction materials, such regolith bricks and structures. Hard structure habitats or inflatable habitats on the Moon still require additional layers for radiation and meteoroid protection, and thermal barrier from direct sun exposure. Such a protection layer can be done with an inflatable structure which is initially laid out to form a habitat configuration. On top of the inflated structure, regolith is piled up from the bottom of the structure and hardened by solar sintering or regolith bricks are stacked up to cover the habitat.

Certain thickness of regolith built on top of the habitats might provide radiation and meteoroid protection capability and at the same time a thermal barrier under the direct exposure of sun light as shown in Figure 30. The measurements and model calculation done without neutron effects by J. Miller et al. [84] indicate that a fairly small amount of regolith, slightly compacted density from 1 to 1.4 g/cm^3, with radiation attenuation depth 46 cm or less, affords substantial protection against primary GCR nuclei (1 GeV) and solar particle event (SPE) protons, with only modest residual dose from surviving charged fragments of the heavy beams. Actual tested data shows the beam energy of 290 MeV/nucleon is completely attenuated after passing 26.6 g/cm^2. Another study shows that regolith is as effective as aluminum to attenuate high energy protons up to 1000 MeV with the thickness of regolith approximately 30 g/cm^2 [85]. This study reveals that the radiation reduction to the limit of 5 Rem (or 50 mSv) requires roughly 150 g/cm^2 or 110 cm thickness of the compacted density 1.4 g/cm^3 [85]. These two studies clearly demand at least 100 cm thick regolith layer to make habitats safe.

There are two ways regolith can be used for radiation shielding: Just like the landing pad work, solar sintering is repeated to develop multilayers of sintered regolith on top of the habitats. The other way is to make bricks of regolith by solar sintering. These regolith bricks are then stacked over the bare frame of habitats. Possibly a new 3-D printing technology can be adopted to make a layer of regolith on top of a habitat. While pouring regolith over a habitat structure in 3-D printing process, the beam of concentrated solar flux follows and heats up the pouring spot of regolith to be sintered.

Figure 30. Cartoonist view of lunar habitat protected by regolith layer coverage from meteoroids and radiation. Image credit [86]

IV-4. Space Radio Telescope for Radio Astronomy

Once the solar sintering as a basic role of solar concentrator is finished, the concentrator can be converted into an antenna for a space radio telescope located on the Moon, as shown in Figure 31. A space radio telescope is an ideal application of solar concentrators, since the Moon does not have ionospheric distortion. The ionosphere on Earth during the solar maximum period is disrupted to generate scintillation that de-correlates the celestial signals among the elements of a ground deployed telescope array. The need of space telescopes is well-described by the following quote: “A space-based low frequency radio instrument would open up the virtually unexplored ultra-long wave (ULW) domain and as such addresses a wealth of science cases that undoubtedly will lead to new exciting scientific discoveries, similar to the uncovering of other wavelength domains has revealed in the past. For most of these science cases such space telescopes would add information to the existing radio, optical, infrared, sub-mm or high frequency X-ray or gamma-ray instrumentation, and thereby providing insight into the processes that take place at the lowest energies and largest physical scales [88].” For such an application,

the parabolic surface of reflector must be refined to meet the resolution requirement which is < 0.5 arc-seconds. Space antenna, unlike telescopes, do not need any baffle structure to shield stray rays or limited use on nighttime. Therefore, it can be located any place on lunar surface to search any radio signals.

The Cassegrain system with optical accuracy will serve as space antenna well without modification of originally implemented functions.

IV-5. Telecommunication Antenna

Super High Performance (SHP) parabolic reflector antenna that is single-polarized and operates at 6.425-20 GHz range is very attractive for telecommunication purpose. Even SHP parabolic reflector antenna is most effective for V-band frequency (40-75 GHz) beyond the Ku (12-18 GHz) and Ka (26.5–40 GHz) bands.

The SHP parabolic reflector antenna can offer ultrahigh performance with exceptional front/back ratio as well as excellent gain. The signal coming from spacecraft, such as Pioneer 10 and 11 and Voyager 1 and 2, at remote location, requires a large aperture antenna to capture the weak signals that comes from far distance away. The Cassegrain system, shown in Figure 20, with 20-meter aperture diameter can be ideally used to capture weak radio signals because the gain of antenna is directly proportional to the aperture area. The gain of a parabolic antenna is defined by

$$\mathrm{G} = \frac{4\pi A}{\lambda^2} e_A = \left(\frac{\pi d}{\lambda}\right)^2 e_A$$

where ***A*** is the area of antenna aperture, *d* the diameter of the parabolic reflector, λ the wavelength of radiowave, and e_A the aperture efficiency. The aperture efficiency of typical parabolic antennas is between 0.55 and 0.7.

Figure 31. Artist view of space antennas on moon. Image credit to NASA [87]

For this radio antenna application, there will not be any additional change or modification necessary from the shape of the initial design for solar concentrator. When the Cassegrain system is developed, an antenna/receiver horn can be built on a turret system that integrates the other three functional instrumentations as such the steering mirror, the gaseous molecule collector, and the image sensor array to capture the optical signals from an object far away. Accordingly, based on a certain role of operation scenarios, this turret system is rotated to set and line up with the optical axis of Cassegrain system.

IV-6. Space Telescope

Agencies of the Department of Defense (DoD) and the National Aeronautics and Space Administration (NASA) have identified airborne and space-based telescope systems that will require mirrors ranging in size from 0.1 to 100 meters in diameter. Since space telescopes in this optical range requires very stringent resolution (< λ/30), the solar concentrator built with flexible membrane may not be qualified to meet the optical resolution due to the difficulty to maintain the design precision. However, it can be used as a base-board platform to build up a high accuracy parabolic reflector by patching segmented optical elements to form a near perfect parabolic mirror, such as the hexagonal mirror segments of the James Webb Space Telescope.

The primary reflector for a large-scale Cassegrain telescope imposes optical and structural design challenges due largely to the resolution requirement (< λ/30) over the likely persisting aberrations (chromatic aberration, spherical aberration, astigmatism, coma, field curvature, and distortion). The surface finish to keep the required resolution is an important task, but not a critical challenge. For the operation of a solar concentrator as a space telescope, it requires a baffle to prevent stray rays from falling through the aperture area. In case of observing a faint object in deep space for high contrast image, the stray rays cause the field of view to have bright background that diminishes contrast ratio of the images. There are four sources of stray

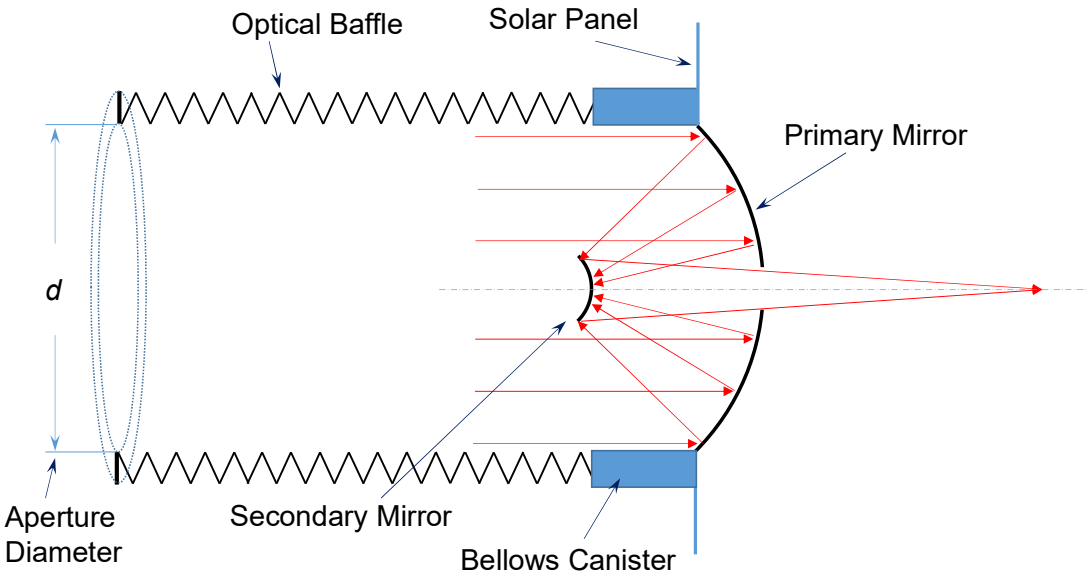

Figure 32. Cassegrain space telescope with optical baffle.

rays – lights emitted or reflected from ground, a bright background sky, reflection from a bright object or multiple reflection of lights within the structure of telescope. For a telescope to operate in the daytime to observe the objects in space, the baffle is a necessary structure to be built around the aperture of a parabolic mirror. Unless the telescope operates on an infrared (IR) range, the baffle can effectively cut off the stray rays. Figure 32 shows a baffle structure that can be deployed from its stow position in canister with gas pressure or mechanical means, just like an accordion pipe.

For space deployment of a large-scale telescope, there are several issues to be addressed: (1) Dimensional constraint with very stringent tolerances, (2) Structural integrity under harsh environment, (3) Weight and volume constraints, (4) Technological barriers, (5) Developmental lead time, and (6) Cost for full development of space telescope.

V. MATERIAL TECHNOLOGY FOR A LARGE-SIZE CASSEGRAIN SYSTEM

For the primary reflector (or mirror) of a lightweight space telescope, monolithic glass and beryllium have been used but reached their limits due to the long lead times, high processing costs, environmental effects and launch load/weight requirements. Materials for mirror technology are a key factor to meet the above limiting issues since new material solutions and manufacturing processes are required to meet the application specific telescope. The primary reflector of a large scale Cassegrain space telescope deals with a low flux density of incident spectral components from far infrared through gamma ray while other government agencies have different mission requirements of mirrors to handle high flux density of photon stream or pulse, for example, DoD's directed energy weapons, reconnaissance/surveillance, and secured communications needs. Over the past several years, silicon carbide (SiC) based materials have been used to fabricate lightweight large-scale mirrors by the United States Air Force, missile defense agency (MDA), and NASA [89-92]. SiC has relatively good thermal stability (60 W/mK/ppm/K) based on thermal conductivity and coefficient of thermal expansion (CTE) versus mechanical stability at 115 GPa/g/cm^3 [89]. With the stability and stiffness of SiC, a structural form of SiC is favorable for many applications that require their operation in harsh environment from cryogenic to high temperatures. Many efforts were done on SiC technology for making mirror structural substrates, figuring and finishing technologies in order to reduce the cost, time, and risks.

Mirror structural substrates made out of advanced engineered materials such as membranes, foams, and composites for ultra-lightweight mirrors are needed and essential for multi-purposed solar concentrator for space antennas, space telescopes, and solar sintering applications. Several material options are contemplated for fabrication of a large scale Cassegrain concentrator.

V-1. Flexible Membrane

Membrane optics have two types of flexible structures: One is based on the Fresnel diffraction principle and the other is based on the gas-filled membrane structure. Fresnel diffraction-based membrane optics offers a shape of flat lens that employs a transparent or reflective plastic panel with diffraction ring gratings. The patterns of Fresnel ring grating are made to focus the incident beam of optical signals through the transmission or reflection. Concentric microscopic grooves are etched into the plastic to provide the diffraction. The

Figure 33. DARPA's concept of a 20-meter folding space telescope. [94]

diffraction patterns are focused on optical axis with spectral distribution along the axis. The longer the wavelength is, the shorter the focal length is. The capture of resolved spectral signals from the Fresnel diffraction requires a certain scrutiny since the spectral focal length is different. The resolution of Fresnel diffraction grating is determined by the number of ring grating [93]. Figure 33 shows the DARPA's concept of a 20-meter transmissive diffractive telescope [94]. The ring grooves and patterned features on one surface, are very tiny in width and height through which light of particular wavelengths is tailored to bend and form wavelength-dependent focal points on optical axis. Since a diffractive light collector focuses the various wavelengths of light at different points on optical axis, it severely limits and diminishes the light signal at any given point of single focal plane. The width and height of these ring grooves on surface are on the order of a few microns. Because light is focused by the diffraction through ring gratings, unlike by refraction produced by bulk glass, Fresnel lenses can be made far thinner and lighter than standard refractive lenses. The disadvantage of diffractive optics–based telescopes is their extremely limited bandwidth. Fortunately, incorporating a second, inverse diffractive lens with a pattern carefully matched to the light collector corrects these focusing aberrations and provides enough photons at the focal plane for imaging.

DARPA's MOIRE program

DARPA plans to use membrane optics as part of its Membrane Optical Imager for Real-Time Exploitation (MOIRE) program. Segmented lightweight polymer membranes are axi-symmetrically arranged on a circular plane to make up a 20-meter diameter. This structure is foldable and capable of seeing a 1-meter object from 36,000 km (22,000 mi) away and video streaming a frame per second. Membrane grooves range from 4 to hundreds of micrometers in width [94].

According to DARPA, glass-based optics in satellites are reaching the point where larger mirrors exceed the lifting power of existing rockets. The MOIRE devices are planned to be one-seventh the weight of a comparable glass-mirrored device.

Individual membranes would be mounted on foldable metal petals as shown in Figure 34. Once in geostationary orbit, the satellite would unfold. The membrane lens occupies one end and a sensor suite the other.

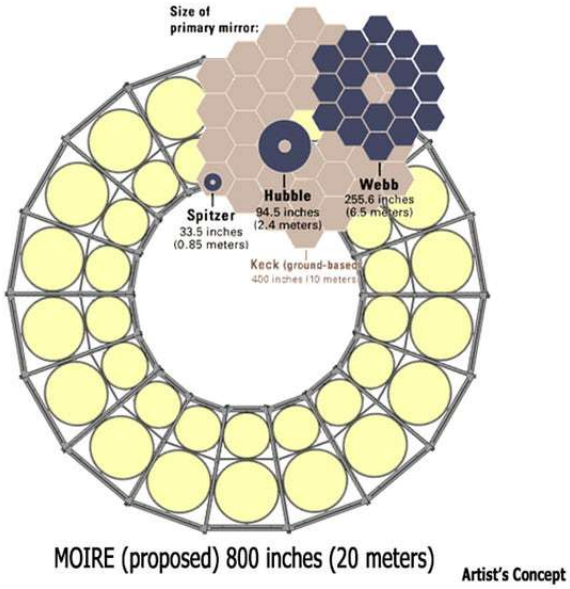

Figure 34. DARPA's MOIRE concept of a 20-meter folding space telescope with size comparison. [94]

The device would be the largest telescope ever built – twice the size of the ground-based twin 10-meter Keck telescopes. It could see about 40 percent of the Earth's surface and could image a 10 km × 10 km area at a 1-metre resolution and generate videos at one frame per second. A ground-based prototype consists of a section of a 5-meter wide device that created the first images with membrane optics.

V-2. Gas-filled Membrane Optics:

The other membrane is the gas inflated flexible reflector. The pre-made shapes are inflated to be convex or concave mirrors by gas pressure [95]. The resolution of gas inflated mirrors is too poor to be used as image capture optics. Patino-Jimenez [95] reported that the inflated mirror shown in Figure 35 can achieve a resolution of 0.1 mm which is very poor as an image collection device. Figure 36 is a sample of inflatable mirror made of flexible polymeric membrane [95]. This type of inflatable reflector can be used for solar concentration, but not suitable for a space telescope, because of poor resolution. The development of inflatable space antenna was initiated at Jet Propulsion Laboratory (JPL) for synthetic aperture radar (SAR) multilayer
microstrip array for Earth remote sensing at the L-band frequency and for the deep-space telecom application of the inflatable microstrip reflectarray at the Ka-band frequency [96]. The boom frames of JPL antennas were initially inflated to set the proper tension on strip array antenna plane to secure the flatness of antenna at the time of deployment and then self-rigidized to fix the tension.

Gas-filled membrane pockets are also vulnerable to slow deflation by gas leak in vacuum. As a short-term remedy, gas carried in a gas tank can refill to compensate the loss of gas pressure, but such a continuous gas leak poses a difficulty to maintain exact pressure. The wave-front

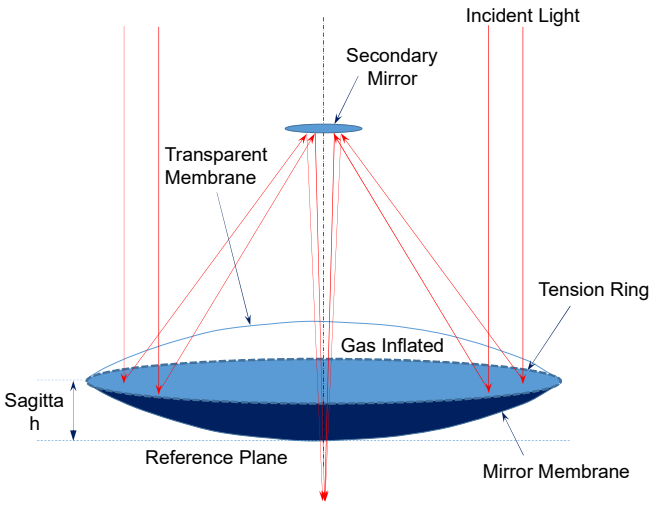

Figure 35. Conceptual view of inflatable mirror made of flexible membranes.

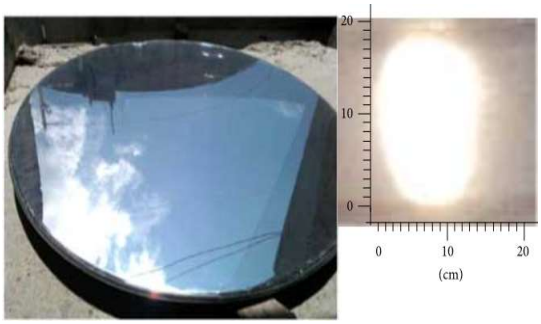

Figure 36. Prototype inflatable mirror made of flexible polymeric membranes. [Figure 8 of ref. 97]

aberration in the inflatable membrane optics is a serious problem. Adoptable correction of wave-front aberration is not well-developed but some efforts have been made recently [97].

Glass transmits light with 90% efficiency, while membrane efficiencies range from 30-55%. Membrane thickness is on the order of that of plastic wrap.

V-3. Composite Foam Structure

The availability of large lightweight materials with low CTE and low Poisson ratio expands continually the realm of missions and applications, especially space telescopes with the great detail of highly resolved spectral information. Future space telescopes and spectral image surveillance/reconnaissance systems would require very large mirrors, from 10 to 17 meters in aperture diameter [98], or even larger [94]. There are two types of space telescope architectures: one is the monolithic primary aperture mirror, the other is a segmented primary mirror, such as JWST. For the segmented mirrors, a segment should be no larger than the diameter of payload fairing. For the upgraded version of the NASA's Space Launch System (SLS) planned for EM-2 in 2021 (SLS Block IB), the payload fairing size of cargo mission is about 8.4 meters in diameter. Accordingly, the maximum size of packaged segmented mirrors should be less than the SLS payload fairing size to fit into a payload bay of launch vehicle shroud [99].

Unlike the architecture of segmented space telescope deployable in space, the multi-purpose segmented telescope to be deployed on the lunar surface requires a substructure with powered wheels to move around by carrying the telescope on top of it, as shown in Figure 20. This movable substructure offers multi-tasking operations of the segmented Cassegrain system for regolith sintering for landing pad and habitats, space antenna, and space telescope. Once landed to a designated location of the lunar surface, these segments would then be assembled or deployed for a specified job among solar sintering, space antenna, or space telescope. To meet the launch payload weight constraints, a mirror segment would also have to be substantially lightweight with an aerial density well below 20 kg/m^2. Since the 20-meter aperture has an area of roughly 400 m^2, the total weight is 8000 kg. If the weight of substructure is 10,000 kg, the total system weight is 18 metric tons. Their reliability and robustness are a major concern because they will be un-shielded and exposed to the high launch loads, on-site assembly damage, and micro-meteor impacts. The successful development of the JWST by NASA will incorporate these types of concepts using cryo-cooled beryllium mirrors that have a projected areal density requirement at the 20-25 kg/m^2 [100]. The JWST is currently scheduled

Figure 37. Syntactic foams. A fine surface finish is possible. (Courtesy CMT Plastic) [107]

to be launched in the 2021 timeframe with capability far exceeding the current Hubble Space Telescope, which has an areal density of the primary mirror of ~180 kg/m^2 [100,101].

Fabrication of large, lightweight, high precision mirrors that are able to maintain the originally designed shapes is most desirable for enhanced surveillance/reconnaissance missions, directed energy weapons and communication systems, laser radar systems, X-ray and UV telescopes, as well as large astronomical telescopes. However, due to the CTE of materials under the temperature gradient, the gravity related load factors, and the aging effect, the mass, size, first modal frequency, and reliability are major design and control issues to ensure the spectral stability of mirrors without causing aberrations. Another aspect of issues are the flight/launch constraints and anticipated life times. New type or new formation of materials that warrant lightweight and high precision optical quality within an acceptable tolerance under dimensional stability of alleviated CTE effect [102] and at the same level meets those specific requirements discussed above are a key point for successful development of mirrors. Numerous foam and composite materials have been studied for various applications [103-106]. Additional consideration for development and fabrication of a large piece foam or composite structure is the cost, production infrastructure, and scheduling which are important technology drivers in some missions where high acreage is required.

Design rules for segmented mirrors, as shown in JWST, depend largely on the overall aperture size of the mirror that determines the spectral resolving power, the deployment option (in space or on Lunar surface), the selection of mirror materials, the requirements of onsite assembly and operation, etc. Regardless of applications, lightweighting of large and high precision mirror is essentially a key objective for space telescope because the weight of the mirror directly affects the size and weight of the support and slewing structures. It is already known that glass mirror materials have reached their minimum weight, so additional weight reduction is only possible by introducing new materials and optimized hybrid material designs.

Figure 37 shows several samples of syntactic foams that are machinable and can have very fine surface features. Casting or fabrication of syntactic foams require the filler materials and the networked mesh structure. If BNNT is selected for composite foam, the polymers, ceramics, or glass can be a filler material to fill the fiber mesh of BNNT.

V-3-1. BNNT based Composite Foam Structure:

V-3-1-1. Boron Nitride Nanotube (BNNT)

One-dimensional nanofiller materials, such as carbon nanotubes (CNTs) and boron nitride nanotubes (BNNTs) offer a new alternative for reinforcing polymers, ceramics, and metals owing to their superior mechanical properties along with their low densities. Nanotubes are unique reinforcing fillers offering not only high modulus and hardness but also high strength and toughness. They are flexible because of their long aspect ratio and do not break up to 30% strain because they can deform adiabatically throughout the entire sp^2 tube network. It has been reported that CNTs can improve modulus, strength, and % elongation at break of poly(p-phenylene benzobisoxazole) (PBO) fiber, which is stronger than Kevlar® [108]. Nanotubes behave like thermoplastic toughers offering various toughening mechanisms including crack path deflection, crack bridging, nanotube pull-out, physical entanglements, to name a few [109]. However, CNTs are easily oxidized in air above 400°C, leading to degradation in mechanical properties of CNTs and little reinforcing effect on high temperature ceramics and metals. BNNTs are new attractive nanotubes owing to their low density (ρ, 1.4 g/cm^3), high mechanical strength

(Young's modulus, E = 0.7-0.9 TPa, yield strength: ~35 GPa experimentally), and excellent chemical stabilities as shown in Table 8. Especially for high temperature applications, superior thermal stability (stable up to 800°C under atmospheric conditions) of BNNTs makes them more suitable for strengthening and toughening ceramics and metals than CNTs. In addition, thermal conductivity (κ) of BNNT is very high above 1000 W/mK theoretically and above 500 W/mK of individual BNNTs have been reported. The coefficient of thermal expansion (α) is also very low approaching 1 x 10^{-6} /K. The Poisson ratio of BNNT is around 0.2, which depends on the length and diameter.

Table 8. Theoretical properties of carbon nanotubes and boron nitride nanotubes.

	Carbon Nanotubes	**Boron Nitride Nanotubes**
Electrical Properties	Metallic or semiconducting	Wide band gap (about 6.0 eV) Insulation, corrosion resistant
Mechanical Properties (Young's Modulus)	1.33 TPa (very stiff)	1.18 TPa (very stiff)
Thermal Conductivity	>3000 W/mK (highly conductive)	~300–3000 W/mK (highly conductive)
Thermal Oxidation Resistance	Stable up to 300-400 °C in air	Stable to over 900 °C in air
Neutron Absorption Cross-Section	C = 0.0035 barn	B = 767 barn (B^{10} ~3800 barn) N = 1.9 barn Excellent radiation shielding
Polarity	No dipole	Permanent dipole Piezoelectric (0.25-0.4 C/m^2)
Surface Morphology	Smooth	Better interfacial strength for composites, ionic bonding
Color	Black	White (can be colored)
Coefficient of Thermal Expansion	-1 x10^{-6} K^{-1} (very low)	-1 x 10^{-6} K^{-1} (very low)

To date, BNNTs have been grown by a number of techniques which can be divided into two broad categories based on the class of material produced and the temperature employed. One is the high temperature synthesis method that vaporized elemental boron from boron (B) or boron nitride (BN) targets react with nitrogen and condense into the solid state. The high temperature methods such as laser heating, arc discharge, or radio frequency (RF) thermal plasma processes produce BNNTs of high quality (few defects and small numbers of walls). The other category of BNNT synthesis is the low temperature synthesis method, applied between 600 and 1700°C, well below the vaporization temperature of pure boron (over 4,000°C, depending on ambient pressure). The low temperature synthesis methods include ball-milling and chemical vapor deposition (CVD), but the quality of BNNTs is much lower than that of the high temperature grown BNNTs [110]. Typical diameters of CVD and ball-milled BNNTs are about an order of magnitude greater than those grown by high temperature synthesis method (~50 nm versus ~5 nm). These tubes frequently suffer from faceted/wavy walls, elbows, herringbone or bamboo-like morphologies. NASA Langley Research Center (LaRC) produced

high quality BNNTs using a novel High Temperature Pressure (HTP) BNNT synthesis method, which has been licensed by a local company to produce large quantities and high quality BNNTs. NASA LaRC has been a lead on BNNT research and collaborating with all the major BNNT producing institutes and companies for many years.

V-3-1-2. BNNT Based Foam Structure

To build a multi-purpose large Cassegrain solar reflector system, lightweight, structurally robust, segmented mirrors with high precision optical quality are required. A number of foam structures have been proposed and used for optical systems in space applications including space telescopes. Nevertheless, there are few materials available to meet the stringent requirements for the space mirrors and reflectors. The candidate materials should have desirable intrinsic properties, which include low density, high modulus/strength, low Poisson's ratio, low coefficient of thermal expansion, high thermal conductivity, low specific heat, high thermal stability, UV resistance, and space radiation resistance. BNNTs are one of the few materials, which can offer all of the demanded properties as shown in Table 8. Additionally, BNNTs provide unique radiation shielding capabilities against galactic cosmic rays (GCR), solar particle events (SPE), and secondary neutron radiation very effectively compared to the other inorganic and metallic candidates, which is a great benefit to be used for long term space missions. Self-deflection (ρ/E) and steady state thermal (α/κ) are important figures of merits to downselect a material for the segmented space mirror systems. The density of BNNT is about 1.4 g/cm^3 and the theoretical modulus is about 1.18 TPa; the self-deflection (ρ/E) is only 1.186, which is at least an order of magnitude smaller than other candidate materials. The Poisson ratio of BNNT is around 0.2, which depends on the length and diameter. The thermal conductivity (κ) of BNNT is very high, above 1000 W/mK theoretically, and greater than 500 W/mK for an individual BNNT has been reported. The coefficient of thermal expansion (α) of BNNT is also very low, approaching 1 x 10^{-6}/K, so the steady state thermal (α/κ) is 0.002 μm/K, which is the lowest among the candidate materials for the multi-purpose Cassegrain solar concentrator. Therefore, BNNTs are excellent potential candidates to build the multi-purpose segmented Cassegrain solar reflector system.

BNNTs are a benign material, not like beryllium, which allows for super-polishing and diamond turning readily without generating hazardous waste. Lightweight BNNTs are very strong and tough, not like SiC, which allows to build a structurally robust large Cassegrain structure against launch vibrations, landing impacts, and meteorite impacts. BNNTs are excellent thermal neutron shielding materials because of the presence of boron, which has a huge neutron absorption cross-section. On the lunar surface, GCRs and SPEs interaction with lunar regolith generates neutrons and other secondary radiation, which makes the lunar surface a more difficult environment for conventional shielding strategies. Figure 38 shows the calculated dose from the combined effects of primary GCRs and the secondary radiation produced when GCRs interact with the lunar regolith [111]. While neutrons are not present in the primary radiation (GCRs or SPEs), a significant neutron flux is produced when the GCRs and SPEs interact with the Moon, Mars, and asteroid surfaces. Therefore, future human lunar landers and habitats need effective shielding materials against not only GCRs and SPEs, but also neutron radiation. BNNT composite based multi-purpose Cassegrain solar concentrators can be used in these space radiation environments for a long-term mission very effectively over other candidate materials. In addition, the BNNT based solar reflector system can serve as a radiation shielding for landers and habitats when needed or as a reusable resource.

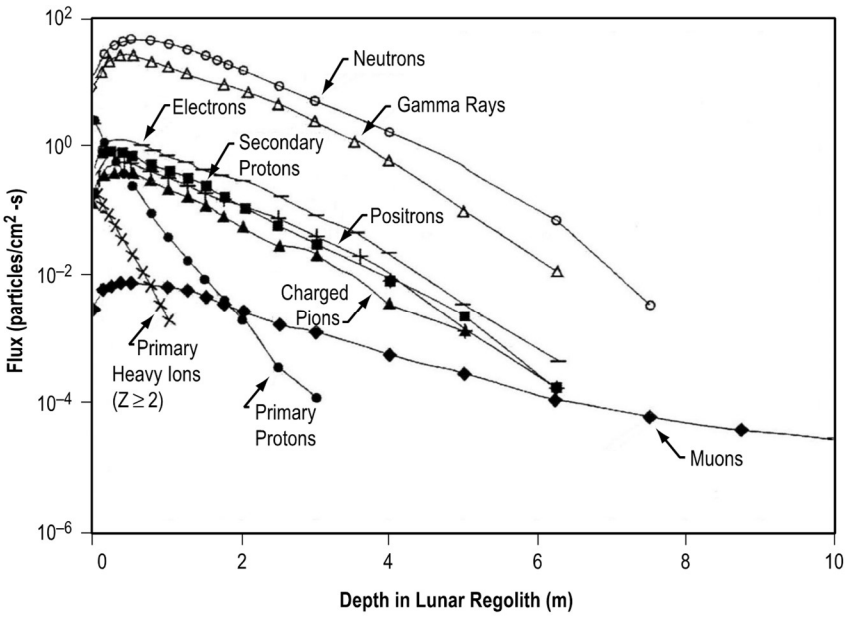

Figure 38. Calculated results for secondary radiation produced when primary galactic cosmic radiation interacts with the lunar regolith [111].

V-4. Segmented Composite structure

The use of BNNT for developing main composite structures is beneficial because of radiation shielding capability and low CTE as tabulated in Table 8. For space applications, composite

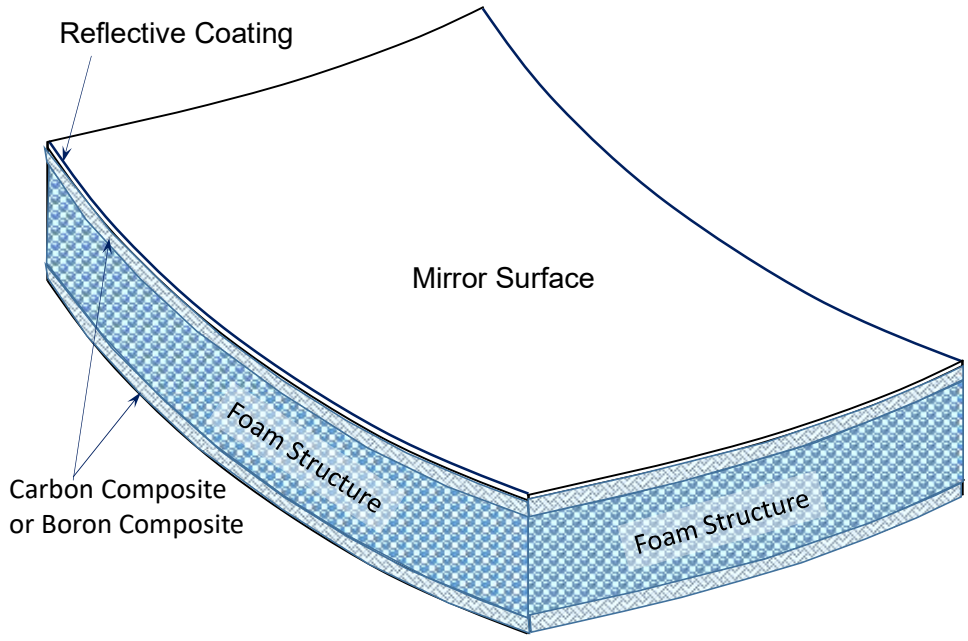

Figure 39. Segmented mirror with composite reinforced syntactic foam.

foam structures should be developed using materials which are light weight while offering mechanical strength. The low CTE of materials, in particular, offer many important applications, such as instrument platform and baseboard for space optics that require stringent shape uniformity with extremely low dimensional variations of composite foam structure even under any surrounding conditions of fast changing environment. Dimensional changes in any structural form is dictated by the CTE and Poisson ratio of BNNT as a key component of composite foam materials. Figure 39 depicts the sketch of a lightweight segmented mirror built with CNT or BNNT composite foam. BNNT is preferred for composite structure since BNNT has much longer strand than CNT, high temperature stability, and better interfacial strength for composites with ionic bonding (see Table 8). The strength of these composites can be explained by three major mechanisms: the superior load transfer for long BNNT reinforcement, the improvement in matrix-nanotube bonding due to trace amount of interfacial product and formation, and the crack bridging by directionally aligned long nanotubes [112].

The 20-meter aperture diameter of solar collector/space telescope appears to be most effective for regolith sintering as shown in Figure 25. As a space telescope with this aperture size, it will offer a formidable optical resolution we have never built in our history. However, there are two folds of key technological challenges to develop such a giant optical instrument: one is the fabrication of light weight and dimensionally stable BNNT composite foam. The other is the design and development of substructure that needs autonomous controllers to sustain the assembly of segmented mirrors intact for the required optical precision. These challenges hinge on the BNNT production technology and the design capability of finely tunable controlled structure. The scientists at NASA Langley Research Center have studied BNNT production and NASA has transferred the technology to a company who plans to develop a method for the mass production of high quality BNNT. A team of material scientists and structural engineers at

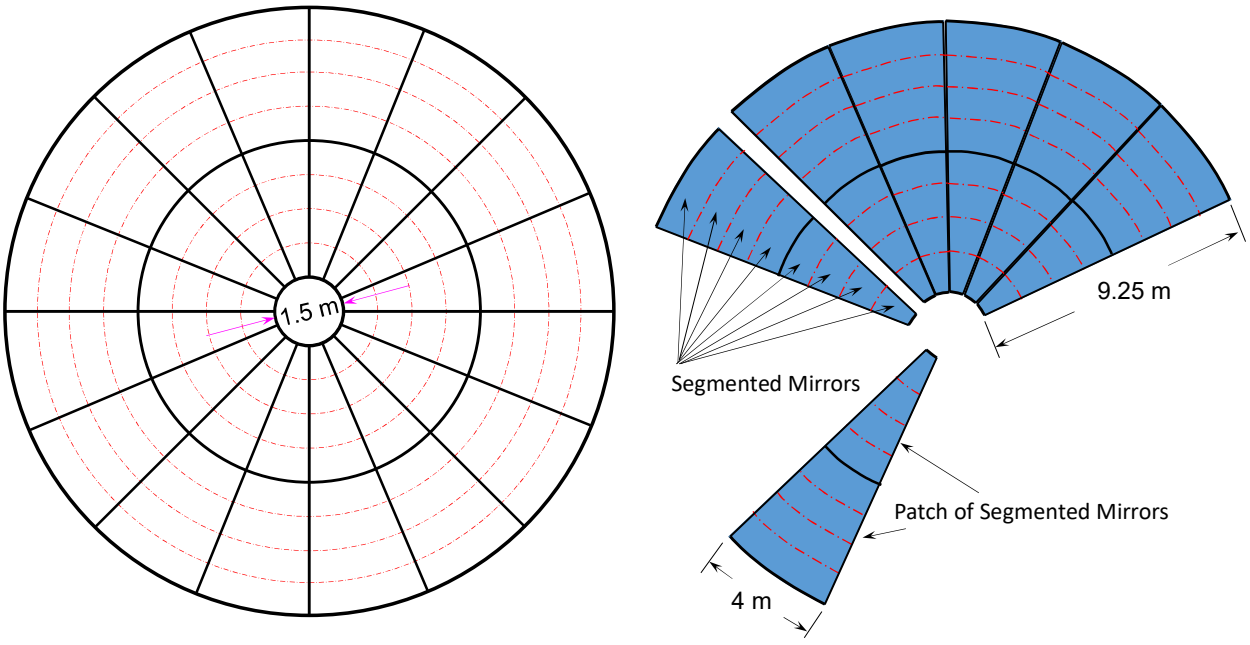

Figure 40. [left] Top view of Cassegrain dish assembled with segmented mirrors. [right] Patch with 4 segmented mirrors.

Langley who have a broad expertise on design and fabrication of space large structures are ready to accept such daunting challenges.

Figure 40 shows the top-down view sketch of a 20-meter Cassegrain system which is composed of segmented mirrors. The Cassegrain reflective mirror is divided into several patches that are comprised of segmented mirrors as shown on the right side of Figure 40. The size of segmented mirrors is determined by the payload fairing of transportation system. The baselined size of a patch of segmented mirrors should be able to fit the Block 2 Cargo payload fairing of NASA's Space Launch System (SLS) as shown in Figs. 41 and 42. The widest side and length of a patch shown in Figure 40 are 4 meters and 9.25 meters. Assume that the

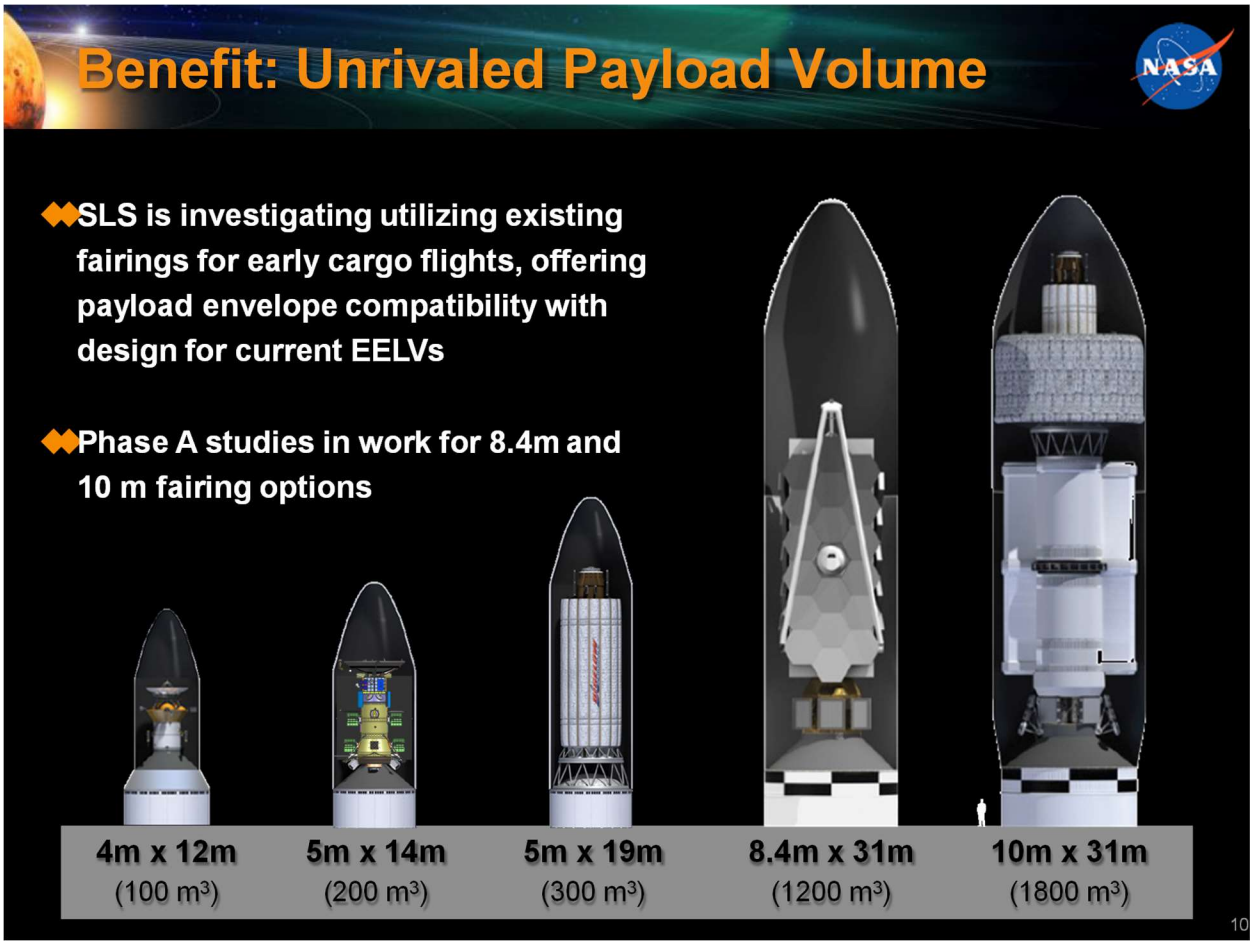

Figure 41. Size and volume of payload fairings of SLS Block 1 and 2. (Credit NASA)

thickness of a segmented mirror and packaging material for secured transportation are 0.1 meter and 0.4 meter. Total thickness per each patch becomes 0.5 meter. Since the Cassegrain system consists of a total of 16 patches, the total package of 16 patches are 8 meters which will fit payload fairing as a single load. Since the foot-print of this payload is actually 4 m by 8 m, the rest of the payload fairing space can be loaded by other substructure frames. The rest of the substructures of Cassegrain system can be delivered as a second payload by SLS Block 2.

Therefore, two launching services by SLS Block 2 will be sufficient for the delivery of Cassegrain system on the Moon's surface.

The deployment of delivered Cassegrain system requires a neat procedure for assembly by robotic manipulation and/or astronauts. Further implementation plan of Cassegrain system for deployment and detailed tasks describing the multi-purpose activities will be continuously studied and reported as a follow-up NASA TM.

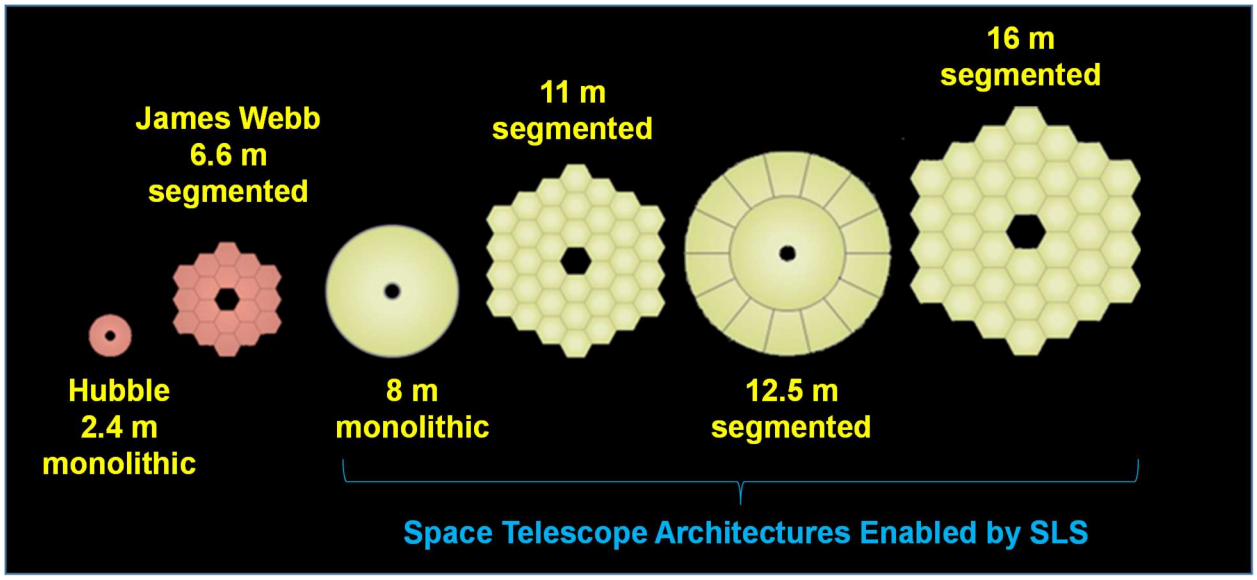

Figure 42. Potential space telescope architectures that can be transported by SLS. (Credit NASA)

VI. CONCLUDING REMARKS

The mission scenarios of NASA's Lunar and Mars explorations are generally well-illustrated over the last several decades. Now main details of mission scenarios are laid out to fulfill meaningful missions beyond the first steps towards Lunar exploration successfully carried out through the Apollo project. One of the challenges for setting a Lunar colony is the delivery of payloads to the surface of Moon but the rocket plume creates a huge cloud of nano to micro scale regolith particles which might be electrostatically charged. To alleviate this regolith cloud formation while landing or launching, solar sintering is necessary to develop a landing pad using air-mass zero (AM0) sunlight and regolith. Also, regolith can cover habitats on the Moon for additional radiation shielding. For solar sintering we considered a Cassegrain solar concentrator. However, the solar sintering job alone is too expensive. To alleviate this cost concern, a multi-purpose use of Cassegrain system was broadly studied here for:

- Solar Sintering: Landing pad and habitat development on Moon
- Harvesting capability of gaseous molecules: H_2O, OH, O_2, H_2, and He-3
- Space Antenna: telecommunication
- Space Telescope: A large scale with 20-meter aperture

To fulfill the tasks listed above, a key and essential technology is the successful construction of segmented mirrors that meet the optical requirements for Cassegrain system. In the harsh lunar environment, the Cassegrain reflector should maintain its optical integrity for telescope performance. NASA Langley developed BNNT appears to be an excellent candidate material to fabricate segmented mirrors since BNNT offers several advantageous material properties, such as the mechanical strength, light weight, low CTE, low Poisson ratio, long BNNT, high thermal conductivity, and radiation shielding capability. Such excellent properties of BNNT are ideal for segmented mirrors of the Moon-based Cassegrain system. Also segmented composite foams of BNNT can be used for construction of habitats like an igloo form.

REFERENCES:

[1] Halekas, J. S., Lin, R. P., and Mitchell, D. L., "Large negative lunar surface potentials in sunlight and shadow", *Geophysical Research Letters*, Vol. 32, Issue 9, pp. 1-4, May 7, 2005. doi:10.1029/2005GL022627

[2] Heiken, G. H., Vaniman, D. T., French, B. M., *The Lunar Sourcebook: A User's Guide to the Moon*, Cambridge University Press, 2005.

[3] Snowden, S. L., Collier, M. R., and Kuntz, K. D., "XMM-Newton Observation of Solar Wind Charge Exchange Emission", *The Astrophysical Journal*, Vol. 610, No. 2: August, 2004, pp, 1182-1190.

[4] Walton, O. R., "Adhesion of Lunar Dust," *NASA CR-2007-214685*, April, 2007, pp. 1-41.

[5] Stubbs, T. J., Vondrak, R. R., and Farrell, W. M., "Impact of Lunar Dust on the Exploration Initiative", *Lunar and Planetary Science Conference XXXVI*, Abstract 2277, League City, Texas, March 14-18, 2005, pp. 1-2.

[6] McCoy, J. E., "Photometric Studies of Light Scattering above the Lunar Terminator from Apollo Solar Corona Photography," *Proceeding of 7th Lunar Science Conference*, Vol. 1, A77-34651 15-91, Houston, Texas, March 15-19, 1976, pp. 1087-1112.

[7] Goodwin, R., "Apollo 17: The NASA Mission Reports," *Vol 1: Apogee Books Space Series*, 29, 2002. ISBN-13: 978-1896522593.

[8] *Heliophysics Science and the Moon*: Potential Solar and Space Physics Science for Lunar Exploration, Report to the NASA Advisory Council Heliophysics Subcommittee, Section 15, September 2007, pp. 1-66. https://ntrs.nasa.gov/archive/nasa/casi.ntrs.nasa.gov/20090010241.pdf

[9] Hintze, P., Curran, J. and Back, T., "Lunar Surface Stabilization via Sintering or the use of Heat Cured Polymers," AIAA-2009-1015, 47th AIAA Aerospace Sciences Meeting Including the New Horizons Forum and Aerospace Exposition, 5-8 January 2009, Orlando, Florida.

[10] Hogue, M. Mueller, R., Sibille, L., Hintze, P., and Rasky, D., "Extraterrestrial Regolith Derived Atmospheric Entry Heat Shields," NASA TR 20150023114, 2016 ASCE Earth & Space Conference; 11-15 April 2016; Orlando, Florida.

[11] Ruess, F., Schaenzlin & Benaroya, H., "Structural Design of a Lunar Habitat". Journal of Aerospace Engineering 19, 2006 133-157.

[12] Advanced Automation for Space Missions" in 1980 NASA/ASEE Summer Study (eds. Freitas Jr., R. A. & Gilbreath, W. P.) 1980.

[13] Mueller, R. P. and King, R.H., “Criteria for Lunar Outpost Excavation,” Space Resources Roundtable –SRR IX, October 26, 2007, Golden, Colorado

[14] Nozette, S., et al., “The Clementine Bistatic Radar Experiment”, Science, Vol. 274, Issue 5292, pp. 1495-1498, 29 Nov 1996, doi: 10.1126/science.274.5292.1495.

[15] Feldman, W.C., et al., “Major compositional units of the Moon: Lunar Prospector thermal and fast neutrons”, Science, 281, 1489-1493, Sept. 1998.

[16] Bussey, D.B.J., Lucey, P.G., Steutel, D., Robinson, M.S., Spudis, P.D., and Edwards, K.D. “Permanent shadow in simple craters near the lunar poles”, Geophysical Research Letters, v. 30 (6), 1278, 2003. doi: 10.1029/2002GL016180.

[17] Neutron Spectrometer Results, Lunar Prospector, Jan. 17, 2009. https://web.archive.org/web/20090117210125/http://lunar.arc.nasa.gov/results/neures.htm

[18] Lucey, P.G., “A Lunar Waterworld”, Science, vol. 326, issue 5952, pp.531-532, Oct. 23, 2009. doi: 10.1126/science.1181471.

[19] Clark, R.N., “Detection of Absorbed Water and Hydroxyl on the Moon”, Science, vol. 326, issue 5952, pp.562-564, Oct. 23, 2009, doi: 10.1126/science.1178105.

[20] Zubrin, R. M., "Moon Direct: A New Plan for a Cost-Effective Luna Base", 2018 AIAA SPACE and Astronautics Forum and Exposition, AIAA SPACE Forum, (AIAA 2018-5110). https://doi.org/10.2514/6.2018-5110

[21] Yeonjoon Park, John D. Wright, Jared D. L. Jensen, Glen C. King, and Sang H. Choi, “Diffraction Analysis for Periodic Nano-scale Apertures, Scatterers and Absorbers”, IOP Journal, Measurement Science and Technology, 16, pp2208-2212, 2005.

[22] Yeonjoon Park, Laura Koch, SangJoon Park, Glen C. King, Kyo D. Song, and Sang H. Choi, “Miniaturization of a Fresnel Spectrometer”, Journal of Optics A: Pure and Applied Optics, Vol. 10, (2008), 095301, doi: 10.1088/1464-4258/10/9/095301.

[23] Yeonjoon Park and Sang H. Choi, “Miniaturization of Optical Spectroscopes into Fresnel Micro Spectrometer”, Commemorative paper, Journal of Nanophotonics, Vol. 7, 077599, 2013.

[24] U.S. Patents: 8,089,677, January 3, 2012; 7,379,231 B2, May 27, 2008; 8,294,989, October 23, 2012; 8,015,815 B2, September 13, 2011; 8,174,695, May 8, 2012; 8,059,273 B2, November 15, 2011; 8,094,306, January 10, 2012.

[25] Min Hyuck Kim, Hargsoon Yoon, Sang H. Choi, Fei Zhao, Jongsung Kim, Kyo D. Song, and Uhn Lee, “Miniaturized and Wireless Optical Neurotransmitter Sensor for Real-time Monitoring of Dopamine in the Brain”, Sensors, Vol. 16, Issue 11, (ISSN 1424-8220; CODEN: SENSC9), Nov. 2016.

[26] Nakagawa, M., et al., “The Moon as a Beach of Fine Powers”, Lunar Regolith Simulant Materials Workshop, Jan. 24-26, 2005.

[27] Heiken, G. H., Vaniman, D. T., French, B. M., The Lunar Sourcebook: A User’s Guide to the Moon, Cambridge University Press, 2005.

[28] Wang, Y. M., “On the Relative Constancy of the Solar Wind Mass Flux at 1 AU”, The American Journal Letters, Vol. 715, 2010, pp. L121-L127, doi:10.1088/2041-8205/715/2/L121.

[29] Summanen, T., Lallement R., and Quemerais, E., “Solar Wind Proton Flux Latitudinal Variations: Comparison between Ulysses in situ Data and Indirect Measurements from Interstellar Lyman alpha Mapping”, Journal of Geophysical Research Space Physics, Vol. 102, No. A4, 1997, pp. 7051-7062. doi: 10.1029/96JA02091.

[30] Kellerman, A. C. and Shprits, Y. Y., “On the Influence of Solar Wind Conditions on the Outer-electron Radiation Belt”, Journal of Geophysical Research, Vol. 117, A05217, 2012. doi: 10.1029/2011JA017253.

[31] Reeves, G. D., Morley, S. K., Friedel, R. H. W, Henderson, M. G., Cayton, T. E., Cunningham, G., Blake, J. B., Christensen, R. A., and Thomsen, D., “On the relationship between Relativistic Electron Flux and Solar Wind Velocity: Paulikas and Blake revisited”, Journal of Geophysical Research, Vol. 116, A02213, 2011. doi: 10.1029/2010JA015735.

[32] McComas, D. J., Funsten, H. O., Guselier, S. A., Lewis, W. S. Mobius, E. Schwadron, and Na. A., “IBEX Observations of Heliospheric Energetic Neutral Atoms: Current Understanding and Future Directions,” Geophysical Research Letters, Vol. 38, L18101, 2011. doi: 10.1029/2011GL048763.

[33] Zimmerman, M. I., Farrell, W. M., Stubbs, T. J., Halekas, J. S., and Jackson, T. L., “Solar Wind Access to Lunar Polar Craters: Feedback between Surface Charging and Plasma Expansion,” Geophysical Research Letters, Vol. 38, L19202, 2011. doi:10.1029/2011GL048880.

[34] Liu, Y. and Taylor, L. A., “Water on the Moon”, Acta Petrologica Sinica, Vol. 27, Issue 2, 2011, pp. 579-588.

[35] Halekas, J. S., Delory, G. T., Brain, D. A., Lin, R. P, Fillingim, M. O., Lee, C. O., Mewaldt, R. A., Stubbs, T. J. Farrell, W. M., and Hudson, M. K., “Extreme Lunar Surface Charging during Solar Energetic Particle Events” Geophysical Research Letters, 34, L02111, 2007. doi:10.1029/2006GL028517.

[36] Mukherjee, N. R., “Solar-wind Interactions with the Moon”, Earth, Moon, and Planets, Vol. 21, Issue 3, Nov, 1979, pp. 307-317. doi: 10.1007/BF00897359.

[37] Saito, Y., Yokota, S., Tanaka, T., Asamura, K., Nishino, M.N., Fujimoto, M., Tsunakawa, H., Shibuya, H., Matsushima, M., Shimizu, H., Takahashi, F., Mukai, T., and Terasawa, T., “Solar Wind Proton Reflection at the Lunar Surface: Low Energy Ion Measurement by MAP-PACE onboard SELENE (KAGUYA)”, Geophysical Research Letters, Vol. 35, L24205, 2008. Pp.1-6. doi:10.1029/2008GL036077

[38] Jordan, J. P., Stubbs, T. J., Zeitlin, C., Spence, H. E., Schwadron, N. A., Zimmerman, M. I., and Farrell, W. M., “On the Intreraction between Highly Energetic Charged Particles and the Lunar Regolith”, 43rd Lunar and Planetary Science Conference, The Woodlands, Texas, March 19-23, 2012.

[39] Ball, P., “Moon too static for astronauts?”, Nature News, 2 February, 2007. doi:10.1038/news070129-16 http://www.nature.com/news/2007/070129/full/news070129-16.html.

[40] Snowden, S. L., Collier, M. R., and Kuntz, K. D., “XMM-Newton Observation of Solar Wind Charge Exchange Emission”, The Astrophysical Journal, Vol. 610, No. 2: August, 2004, pp, 1182-1190.

[41] Aellig, M. R., and Lazarus, A. J., “The Solar Wind Helium Abundance: Variation with Wind Speed and the Solar Cycle”, Geophysical Research Letters, Vol. 28, No. 14, Jul. 15, 2001, pp. 2767-2770. doi: 10.1029/2000GL012771.

[42] Abbas, M. M., Tankosic, D., Craven, P. D., Spann, J.F., LeClair, A., and West, E. A., “Lunar Dust Charging by Photoelectric Emissions”, Planetary and Space Science, Vol. 55, No. 7-8, 2007, pp. 953-965. doi: 10.1016/j.pss.2006.12.007.

[43] Stemovsky, Z., Chamberlin, P., Horanyi, M., Robertson, S., and Wang, X., “Variability of the Lunar Photoelectron Sheath and Dust Mobility due to Solar Activity”, J. of Geophysical Research, Vol. 113, A10104, 2008. doi: 10.1029/2008JA013487.

[44] Abbas, M. M., Tankosic, D., Craven, P. D., Spann, J. F., LeClair, A. C., West, F. A., Taylor L., and Hoover, R., “Importance of Measurements of Charging Properties of Individual Submicron Size Lunar Dust Grains”, NASA Whitepaper for the Planetary Science Decadal Survey, NTRS 20050237054, 2005.

[45] Abbas, M. M., Tankosic, D., Craven, P. D., LeClair, A. C., and Spann, J. F., “Lunar Dust Grain Charging by Electron Impact: Complex Role of Secondary Electron Emissions in Space Environment”, The Astrophysical Journal, Vol. 718, No. 2, July 2010, pp. 795-809. doi:10.1088/0004-637X/718/2/795.

[46] Halekas, J. S., Delory, G. T., Lin, R. P., Stubbs, T. J., and Farrell, W. M., “Lunar Prospector Measurements of Secondary Electron Emission from Lunar Regolith”, Planetary and Space Science, Vol. 57, 2009, pp. 78-82. doi: 10.1016/j.pss.2008.11.009.

[47] Forward, K. M, Lacks, D. J., and Sankaran, R. M., “Triboelectric charging of lunar regolith simulant”, Journal of Geophysical Research Space Physics, Vol. 114, A10109, 2009, pp. 3. doi:10.1029/2009JA014559.

[48] Stubbs, T. J., Vondrak, R. R., and Farrell, W. M. , “Impact of Dust on Lunar Exploration”, Proceedings of Dust in planetary systems, Kauai, Hawaii, 2005, pp. 26-30.

[49] Bedingfield, K. L., Leach, R. D., and Alexander, M. B., “Spacecraft System Failures and Anomalies Attributed to the Natural Space Environment,” NASA Reference Publication, 1390, August 1996.

[50] Rennilson, J. J. and Criswell, D. R., “Surveyor's Observations of Lunar Horizon-Glow,” The Moon, 10: 1974, pp. 121-142. doi:10.1007/BF00655715.

[51] Choi, S.H., Elliott, J.R., and King, G.C., “Electrostatic Power Generator with Capacitive Charge Collectors,” NASA Invention Disclosure, Case No. LAR 17516-1, November 28, 2006. ID: 5022945.

[52] Choi, S.H., King, G.C., Kim, H-J, and Park, Y., "Lunar Soil Electrostatic Power Generation & Dust Mitigation", AIAA Paper 815014, Anaheim, CA, Aug. 31~Sep. 2, 2010.

[53] Van de Graaff, R. J.; Compton, K. T.; Van Atta, L. C. "The Electrostatic Production of High Voltage for Nuclear Investigations," Physical Review Vol. 43, No. 3, 1933, pp. 149–157.

[54] Xie, Y, Bos, D., de Vreede, L. J., de Boer, H. L., van der Meulen, M., Versluis, M., Sprenkels, A. J., van den Berg, A., and Eijkel, J. C. T., "High-efficiency ballistic electrostatic generator using microdroplets." Nature Communications, Vol. 5, No. 3575, April 2014, pp. 1-5. doi: 10.1038/ncomms4575.

[55] Boland, J., “Micro Electrolet Power Generators.” Ph.D. Thesis, California Institute of Technology, Pasadena, CA, 2005. p. 56. Fig. II-5.

[56] Kim, B. H., Bamhart, B. S., and Kwon, J. W., “Electrostatic power generation using carbon-activated cotton thread on textile.” Micro and Nano Systems Letters, Vol. 3, No. 3, 2015, pp.1-7. doi: 10.1186/s40486-015-0016-0.

[57] Breaux, O. P., “Electrostatic Power Generation for Space Propulsion,” Electrical Engineering, Vol. 78, Issue 11, 1959, pp. 1102-1104. doi: 10.1109/EE.1959.6446032.

[58] Hyde, W. W., “Electrostatic energy field power generating system,” U.S. Patent: 4,897,592. Jan 30, 1990.

[59] Soliman, M. S. M., El-Saadany, E. F., and Mansour, R. R., “Electromagnetic and Electrostatic Micro-Power Generators; an Overview,” Proceedings of the IEEE, International Conference on Mechatronics & Automation, Niagara Falls, Canada, July 2005, pp. 89-93.

[60] Dhakar, L., “Triboelectric Devices for Power Generation and Self-Powered Sensing Applications, Section 2.1,” Springer Theses, 2017, page 15. ISBN 978-981-10-3815-3, doi: 10.1007/978-981-10-3815-0.

[61] Taylor, L. A., Schmitt, H. H., Carrier III, W. D., and Nakagawa, M., “The Lunar Dust Problem: From Liability to Asset.” 1st Space Exploration Conference: Continuing the Voyage of Discovery, AIAA 2005-2510, Orland, Florida, Feb. 2005, doi:10.2514/6.2005-2510.

[62] Calle, C. I., Buhler, C. R., Johansen, M. R., Hogue, M. D., and Snyder, S. J., “Active dust control and mitigation technology for lunar and Martian exploration,” Acta Astronautica, Vol. 69, 2011, pp.1082-1088. doi:10.1016/j.actaastro.2011.06.010.

[63] Gaier, J. R., Journey, K., Christopher, S., and Davis, S., “Evaluation of Brushing as a Lunar Dust Mitigation Strategy for Thermal Control Surfaces,” 41st International Conference on Environmental Systems, AIAA 2011-5182, Portland Oregon, July 2011, doi:10.2514/6.2011-5182Hansen, J.R., “The Big Balloon: How Project Echo taught NASA the value of a glitch,” Air & Space, vol. 9, no. 1, pp. 70–77, April/May 1994.

[64] Wilson, A., “A History of Balloon Satellites,” Journal of the British Interplanetary Society, vol. 34, pp. 10–22, January, 1981.

[65] Freeland, R.E., Orbital Construction Demonstration Study, Final Report, NAS 9-14916, prepared by Grumman Aerospace Corp for Johnson Space Center, Houston, Texas, June 1977.

[66] Freeland, R.E., Final Report for Study of Wrap Rib Antenna Design, LMSC D714613, Contract No. 955345, prepared by Lockheed Missiles and Space Company for Jet Propulsion Laboratory, Pasadena, California, December 12, 1979.

[67] Freeland, R.E., et al. “Inflatable Space Structures Technology Development for Large Radar Antennas, IAC Paper 04-IAF-I.1.10, 55th IAF Congress (October 4–8, 2004, Vancouver, Canada), International Astronautical Federation, Paris, France, 2004.

[68] Switchboard in the Sky, https://www.nasa.gov/centers/glenn/about/fs13grc.html

[69] Abt, B., Helwig, G., and Scheulen, D., “Highly Precise Reflectors and Mirrors in Fibre-Composite Technology”, Proceedings of an ESO Conference on Very Large Telescopes and their Instrumentation, held in Garching, March 21-24, 1988.

[70] Matter, J., The Next Generation Space Telescope (NGST), Springer, ISBN: 978-94-010-6300-5, In: Eiroa C., Alberdi A., Thronson H., De Graauw T., Schalinski C.J. (eds)

Infrared Space Interferometry: Astrophysics & the Study of Earth-Like Planets. Astrophysics and Space Science Library, vol 215. Springer, Dordrecht.

[71] Bonanno, A.C., Li, A., and Bernold, L., "Comparative Specific Heat Capacity Analysis for Lunar In-Situ Manufacture of Thermal Energy Storage", Earth and Space 2014. https://doi.org/10.1061/9780784479179.046

[72] Colozza, A.J., "Analysis of Lunar Regolith Thermal Energy Storage," NASA CR 189073, Nov. 1991.

[73] Mitchell, J. K., W. N. Houston, R. F. Scott, N. C. Costes, W. D. Carrier III, and L. G. Bromwell (1972a), Mechanical properties of lunar soil: Density, porosity, cohesion, and angle of friction, Proc. Lunar Sci. Conf., 3rd, 3235–3253, 1972.

[74] NASA Invention LAR-19532-1, 2018.

[75] Datta, S., *Electronic Transport in Mesoscopic Systems*, Cambridge University Press, 1995, ISBN: 0-521-41604-3.

[76] Bandfield, J.L., Poston, M.J., Klima, R.L., and Edwards, C.S., "Widespread distribution of OH/H_2O on the lunar surface inferred from spectral data", Nature Geoscience 11, pp.173-177, 2018.

[77] Slyuta, E.N., Abdrakhimov, A.M., and Galimov, E.M., "The Estimation of Helium-3 Probable Reserves in Lunar Regolith", Lunar and Planetary Science XXXVIII, 2007. https://www.lpi.usra.edu/meetings/lpsc2007/pdf/2175.pdf

[78] Lasker, J., "Race to the Moon for Nuclear Fuel", Science, Space. Dec. 15, 2006.

[79] Pontin, M.W., "Mining the Moon", MIT Technology Review, Aug. 23, 2007. https://www.technologyreview.com/s/408558/mining-the-moon/

[80] Shea, D.A. and Morgan, D., "The Helium-3 Shortage: Supply, Demand, and Options for Congress", Congressional Research Service (CRS) Report for Congress #7-5700, R41419, Dec. 22, 2010.

[81] Anderson, S.T., "Economics, Helium, and the U.S. Federal Helium Reserve: Summary and Outlook", Natural Resources Research, Vol. 27, No. 4, pp.455-477, Oct. 2018. doi: 10.1007/s11053-017-9359-y.

[82] Lockley, A., "Helium-3 prices are out of this world", Exponential Investor, Oct. 11, 2017. https://www.exponentialinvestor.com/commodities/helium-3-prices-are-out-of-this-world/

[83] Coustenis, A. and Taylor, F.W., *Titan: Exploring an Earthlike World*, 2nd. Edition, World Scientific Publ., ISBN 978-981-270-501-3. 2008.

[84] Miller, J., et al., "Lunar soil as shielding against space radiation", Radiation Measurements, 2009. doi:10.1016/ j.radmeas.2009.01.010.

[85] Pham, T.T. and El-Genk, M.S., "Regolith Biological Shield for a Lunar Outpost from High Energy Solar Protons", AIP Conference Proceedings 969, Iss. 1, p.474, 2008. https://doi.org/10.1063/1.2845005

[86] Constructing a Lunar Habitats; https://www.youtube.com/watch?v=Ye6xdF8ZBwc

[87] Rawlings, P., "Space Antenna on Lunar Crater", Artwork for NASA, S95-01561, February 1995. https://www.spaceflight.nasa.gov/gallery/images/mars/lunaractivities/html/s95_01561.html

[88] Rajan, R. T., Boonstra, A. J., Bentum, M., Klein-Wolt, M., Belien, F., Arts, M., Saks, A., and van der Veen, A.J., "Space-based Aperture Array for Ultra-Long Wavelength Radio Astronomy", Experimental Astronomy, No. 41, Iss. 1-2, p.271, Feb. 2016.

[89] Matson, L.E., Chen, M.Y., deBlonk. B., and Palusinski, I.A., "Silicon Carbide Technologies for Lightweighted Aerospace Mirror", Advanced Maui Optical and Space Surveillance Technologies Conference, Maui, Hawaii, Sep.16-19, 2008.

[90] Zhang, G., et al. "Fabricating large-scale mirrors using reaction-bonded silicon carbide", SPIE Newsroom, 2016. doi: 10.1117/2.1201607.006582.

[91] Williams, S. and Deny, P., "Overview of the production of sintered SiC optics and optical sub-assemblies, Proc. SPIE 5868, p. 586804, 2005. doi:10.1117/12.617824.

[92] Ealey, M. A., Wellman, J. A., and Weaver, G., "CERAFORM SiC: roadmap to 2m and 2kg/m^2 areal density, Proc. SPIE CR67, pp. 53–57, 1997.

[93] Park. Y. and Choi, S. H., "Miniaturization of Optical Spectroscopes into Fresnel Micro Spectrometer", Commemorative paper, Journal of Nanophotonics, Vol. 7, 077599, 2013.

[94] "DARPA Membrane Optical Imager for Real-time Exploitation (MOIRE) giant folding space telescope", Photonics Media, Dec. 9, 2013. https://www.ball.com/aerospace/programs/moire

[95] Patino-Jimenez, F. et al., "Construction and Optical Testing of Inflatable Membrane Mirror Using Structured Light Technique", Int. J. of Photoenergy, Vol. 2015, Article ID 196186, June 9, 2015.

[96] Huang, J., "The Development of Inflatable Array Antennas," IEEE Antennas and Propagation Magazine, vol. 43, pp. 44–50, August 2001.

[97] Yang, B., et al., "Correcting the wavefront aberration of membrane mirror based on liquid crystal spatial light modulator", SPIE Proceedings 9272, Optical Design and Testing VI, 927218 (5 November 2014); doi: 10.1117/12.2071315.

[98] Postman, M., et al., "Advanced Technology Large-Aperture Space Telescope (ATLAST): A Technology Roadmap for the Next Decade", RFI submitted to NRC ASTRO-2010 Decadal Committee, arXiv:0904.0941 or Bibcode:2009arXiv0904.0941.

[99] Skran, D.L., "Battle of the Collossi: SLS vs Falcon Heavy", The Space Review, April 27, 2015. http://www.thespacereview.com/article/2737/1.

[100] Stahl, H.P., "Optic Needs for Future Space Telescopes", SPIE Proceedings 5180, pp1-5, 2003.

[101] Stahl, H.P., "Large Space Optics: from Hubble to JWST and Beyond", https://ntrs.nasa.gov/archive/nasa/casi.ntrs.nasa.gov/20090014723.pdf.

[102] Chen, M. Y., et al., "Replication of Lightweight Mirrors", SPIE Proceedings 7425, Optical Materials and Structures Technologies IV, 74250S (21 August 2009); doi:10.1117/12.828567

[103] Gupta, N., et al., "Applications of Polymer Matrix Syntactic Foams", J. of Materials, Vol. 66, No. 2, pp.245-254, 2014. doi: 10.1007/s11837-013-0796-8.

[104] Porfiri, M. and Gupta, N., "Effect of Volume Fraction and Wall Thickness on the Elastic Properties of Hollow Particle Filled Composites," Compos. B Eng. Vol. 40, No. 2, 166, 2009.

[105] Shan, Y., et al., “Strength Analysis of Syntactic Foams Using a Three-Dimensional Continuum Damage Finite Element Model,” J. of Applied Mechanics, Vol. 82, Iss. 2, Feb. 2015. doi: 10.1115/1.4029387.

[106] Gupta, N., Pinisetty, D., and Shunmugasamy, V. C., *Reinforced Polymer Matrix Syntactic Foams*, Springer Nature, 2017.

[107] https://cmtmaterials.com/.

[108] Kumar, S., et al., “Synthesis, Structure, and Properties of PBO/SWNT Composites”, Macromolecules, Vol. 35, Iss. 24, pp.9039-9043, Oct. 5, 2002.

[109] Lovell, C. S., et al., “Thermodynamic approach to enhanced dispersion and physical properties in a carbon nanotube/polypeptide nanocomposite”, Polymer Vol. 50, Iss. 8, pp. 1925-1932, April 9, 2009.

[110] Smith, M. W., et al., “Very long single- and few-walled boron nitride nanotubes via the pressurized vapor/condenser method”, Nanotechnology, Vol. 20, No. 50, Nov. 12, 2009.

[111] Armstrong, T.W. and Colborn, B.L. Cosmic Ray and Secondary Particle Environment Analysis for Large Lunar Telescope Instruments. Science Applications International Corporation Report SAIC-TN-912, May 1991.

[112] Nautiyal, P., et al., “Directionally Aligned Ultra-long Boron Nitride Nanotube Induced Strengthening of Aluminum-Based Sandwich Composite”, Advanced Engineering Materials, Vol. 18, No. 10, pp. 1747-1754, 2016. doi: 10.1002/adem.201600212.

REPORT DOCUMENTATION PAGE

Form Approved
OMB No. 0704-0188

1. REPORT DATE *(DD-MM-YYYY)*	2. REPORT TYPE	3. DATES COVERED *(From - To)*
1-10-2020	Technical Memorandum	10-01-2019 - 9-30-2020

4. TITLE AND SUBTITLE

Implementation Concept of Operation for a Multi-Purpose Cassegrain Solar Concentrator, Micro-Spectrometers, and Electrostatic Neutralizers to Enable In-Situ Construction Activities plus Lunar, Planetary, and Deep Space Science Exploration on the Moon

5a. CONTRACT NUMBER

5b. GRANT NUMBER

5c. PROGRAM ELEMENT NUMBER

6. AUTHOR(S)

Sang H. Choi
Robert W. Moses
Cheol Park
Catharine C. Fay
David R. Komar

5d. PROJECT NUMBER

5e. TASK NUMBER

5f. WORK UNIT NUMBER

432938.09.01.07.05.01

7. PERFORMING ORGANIZATION NAME(S) AND ADDRESS(ES)

NASA Langley Research Center
Hampton, VA 23681-2199

8. PERFORMING ORGANIZATION REPORT NUMBER

9. SPONSORING/MONITORING AGENCY NAME(S) AND ADDRESS(ES)

National Aeronautics and Space Administration
Washington, DC 20546-0001

10. SPONSOR/MONITOR'S ACRONYM(S)

NASA

11. SPONSOR/MONITOR'S REPORT NUMBER(S)

NASA-TM-20205009040

12. DISTRIBUTION/AVAILABILITY STATEMENT

Unclassified
Subject Category
Availability: NASA STI Program (757) 864-9658

13. SUPPLEMENTARY NOTES

14. ABSTRACT

This report illustrates a Cassegrain solar concentrator that has multi-functional capabilities for space missions. Proper design and implementation of high-performance lightweight composite materials for the primary mirror of the Cassegrain concentrator can offer multiple capabilities to be performed on the Moon. The multiple applications studied with Cassegrain concentrators are (1) Solar sintering for landing pad and habitats, (2) Harvest of volatiles: H2O, O2, H2, and He-3, (3) Space antenna for telemetry and telecommunication, and (4) Space telescope with 20-meter aperture that exceeds the space telescopes to date in terms of the State-of-Art (SOA) in resolution and aperture diameter.

15. SUBJECT TERMS

Cassegrain concentrators, Solar sintering for landing pad and habitats, Harvest of volatiles, Space antenna for telemetry and telecommunication, and Space telescope

16. SECURITY CLASSIFICATION OF:			17. LIMITATION OF ABSTRACT	18. NUMBER OF PAGES	19a. NAME OF RESPONSIBLE PERSON
a. REPORT	b. ABSTRACT	c. THIS PAGE			STI Help Desk (email: help@sti.nasa.gov)
U	U	U	UU	59	19b. TELEPHONE NUMBER *(Include area code)* (757) 864-9658